J. Fluid Mech. (2012), *vol.* 690, *pp.* 288–320. © Cambridge University Press 2011
doi:10.1017/jfm.2011.430

Vortex events in Euler and Navier–Stokes simulations with smooth initial conditions

P. Orlandi[1]†, S. Pirozzoli[1] and G. F. Carnevale[1,2]

[1] Dipartimento di Ingegneria Meccanica e Aerospaziale, Università La Sapienza, via Eudossiana 16, I-00184, Roma

[2] Scripps Institution of Oceanography, University of California, San Diego, La Jolla, CA, USA

(Received 27 December 2010; revised 26 August 2011; accepted 28 September 2011; first published online 23 November 2011)

We present high-resolution numerical simulations of the Euler and Navier–Stokes equations for a pair of colliding dipoles. We study the possible approach to a finite-time singularity for the Euler equations, and contrast it with the formation of developed turbulence for the Navier–Stokes equations. We present numerical evidence that seems to suggest the existence of a blow-up of the inviscid velocity field at a finite time (t_s) with scaling $|u|_\infty \sim (t_s - t)^{-1/2}$, $|\omega|_\infty \sim (t_s - t)^{-1}$. This blow-up is associated with the formation of a k^{-3} spectral range, at least for the finite range of wavenumbers that are resolved by our computation. In the evolution toward t_s, the total enstrophy is observed to increase at a slower rate, $\Omega \sim (t_s - t)^{-3/4}$, than would naively be expected given the behaviour of the maximum vorticity, $\omega_\infty \sim (t_s - t)^{-1}$. This indicates that the blow-up would be concentrated in narrow regions of the flow field. We show that these regions have sheet-like structure. Viscous simulations, performed at various Re, support the conclusion that any non-zero viscosity prevents blow-up in finite time and results in the formation of a dissipative exponential range in a time interval around the estimated inviscid t_s. In this case the total enstrophy saturates, and the energy spectrum becomes less steep, approaching $k^{-5/3}$. The simulations show that the peak value of the enstrophy scales as $Re^{3/2}$, which is in accord with Kolmogorov phenomenology. During the short time interval leading to the formation of an inertial range, the total energy dissipation rate shows a clear tendency to become independent of Re, supporting the validity of Kolmogorov's law of finite energy dissipation. At later times the kinetic energy shows a $t^{-1.2}$ decay for all Re, in agreement with experimental results for grid turbulence. Visualization of the vortical structures associated with the stages of vorticity amplification and saturation show that, prior to t_s, large-scale and the small-scale vortical structures are well separated. This suggests that, during this stage, the energy transfer mechanism is non-local both in wavenumber and in physical space. On the other hand, as the spectrum becomes shallower and a $k^{-5/3}$ range appears, the energy-containing eddies and the small-scale vortices tend to be concentrated in the same regions, and structures with a wide range of sizes are observed, suggesting that the formation of an inertial range is accompanied by transfer of energy that is local in both physical and spectral space.

Key words: Navier–Stokes equations, turbulence simulation, vortex dynamics

† Email address for correspondence: orlandi@kolmogorov.ing.uniroma1.it

https://doi.org/10.1017/jfm.2011.430 Published online by Cambridge University Press

1. Introduction

A fundamental unsolved problem of fluid dynamics is whether the Navier–Stokes equations can lead to a finite time singularity (FTS) starting from smooth initial conditions. Directly related to this problem is the question of the possible blow-up of the Euler equations. A resolution of these problems will lead to a more complete understanding of turbulence. It will shed light on the complex interaction among the whole range of scales in viscous and inviscid flows, and the energy cascade process, which occurs for both the Navier–Stokes and Euler equations.

Numerical studies of statistically stationary turbulent flow typically employ a fluctuating large-scale forcing. Under these conditions a statistical stationary state is reached and a large amount of data can be accumulated and used to evaluate high-order statistics. Some of the most refined direct numerical simulations (DNSs) of this type were performed by Ishihara *et al.* (2007). The energy spectra that result can be decomposed into regions: the forced low wavenumbers, the adjacent energy containing scales, an intermediate range where the spectrum follows a power law and a small-scale dissipation range where the spectrum falls off exponentially. The energy-containing scales are of interest in turbulence control, but their statistics are not universal. The study of Ishihara *et al.* (2007) focused on the statistical properties of the intermediate and small scales which are not strongly affected by the forcing. Examining simulations at different R_λ (where $R_\lambda = u_{rms}\lambda/\nu$ indicates the Reynolds number based on the Taylor microscale $\lambda = \sqrt{(15\nu u_{rms}^2/\varepsilon)}$) they observed that in the energy spectrum the width of the power law region does not increase with R_λ. They demonstrated that the rate of energy dissipation is limited as R_λ increases, as was postulated by Kolmogorov (1942). Such studies are very illuminating from the point of view of turbulence statistics, but do little to elucidate the role of the viscosity on the vortex dynamics that produce a turbulent flow. To explore that issue it is more useful to study unforced flows with smooth (i.e. not randomly generated) initial conditions.

In laboratory experiments of decaying turbulence, the large-scale structures that drive the turbulence are created by grids. Depending on the flexibility of the grid, different decay rates have been observed (Lavoie, Djenidi & Antonia 2007). Furthermore, by using a fractal grid, Mazellier & Vassilicos (2010) experimentally observed a turbulent behaviour without Richardson–Kolmogorov cascade, consisting of an exponential rather than a power-law decay for the turbulent energy. From these observations it can be asserted that the initial conditions can strongly affect the evolution of the energy spectrum. Control of the energy containing scales in laboratory experiments is rather difficult if not almost impossible. Such control is important if the precise form of the energy containing scales can affect the rest of the spectrum. Perfect control of these scales is simple in numerical simulations.

There have been very few studies of the generation of turbulent flows starting from well-defined vortical flows. One of the more interesting such studies was that by Brachet *et al.* (1983) studying the effects of the viscosity on the evolution of a Taylor–Green vortex. Even using the highest numerical resolution possible for computers available at that time, that study could not investigate several important aspects of turbulence, in particular those related to enstrophy evolution, for the lack of sufficient resolution. Subsequent simulations of this flow were performed by Cichowlas & Brachet (2005) in the inviscid case. From their results, they concluded that a FTS does not occur. Their criterion for the existence of a FTS is based on the behaviour of the logarithmic decrement $\delta(t)$ and the power-law exponent n, assuming that the energy spectrum can be represented at least approximately by $E(k) \approx k^n \exp(-2\delta(t)k)$. The requirement for a FTS is then that $\delta(t)$ tends to zero faster than n tends to the

https://doi.org/10.1017/jfm.2011.430 Published online by Cambridge University Press

value -3. The value $n = -3$ is a critical value because with $\delta = 0$ the enstrophy is finite for all $n < -3$ but becomes infinite if $n \geqslant -3$. Thus, a likely scenario is that a blow-up in finite time will involve both δ vanishing and $n \to -3$ in a finite time. In inviscid flow, the evolution of the logarithmic decrement $\delta(t)$ reflects the fact that it takes time for nonlinear effects to transfer energy from the large scales where it is initially concentrated to the smallest scales. For the Taylor–Green vortex, the evolution of $\delta(t)$ is relatively slow and it is difficult to simulate long enough to observe behaviour suggesting a singularity. Orlandi (2009) suggested that one reason for the negative conclusion of Cichowlas & Brachet (2005) was that their simulation was terminated during a period in which the enstrophy amplification necessary for a singularity was in a premature stage. Orlandi & Carnevale (2007) and Orlandi (2009) have shown that the length of time needed to reach a FTS can be reduced by judicious choice of initial conditions. Also, it should be noted that the behaviour of the energy spectrum near the maximum wavenumber cut-off is linked to the numerical method used, and this may affect the calculation of $\delta(t)$. When pseudospectral methods are used, as in Cichowlas & Brachet (2005), numerical artifacts such as a pile-up of energy near the maximum wavenumber k_{max} may form making it difficult to accurately measure $\delta(t)$. In this regard, there is some advantage to using a finite difference scheme since this kind of pile-up is much reduced. It is fair to say, however, that this shortcoming of pseudospectral methods implementing the classical two-thirds rule can be in principle circumvented through the use of high-order exponential filters (Hou & Li 2006; Bustamante & Kerr 2008). With both energy-conserving finite-difference and pseudospectral numerical methods, in the event of a FTS, the simulations can be extended past the FTS, after which time we would expect to see an unphysical equipartitioning of energy tending toward a k^2 spectrum near k_{max}.

In an attempt to create conditions ideal for studying the possibility of a FTS, Kerr (1993) used an initial condition in which two antiparallel vortices with Gaussian cores were perturbed so that they would interact strongly. Kerr (1993) notes that his initial conditions involve some spectral filtering to avoid oppositely signed vorticity regions around the main cores that prevent singular behaviour. Kerr (1993) presents evidence that these initial conditions tend to evolve towards a FTS. More recent attempts to search for this FTS by Hou & Li (2006) with the same initial conditions, however, gave evidence that a FTS does not occur. Using highly resolved pseudospectral simulations with exponential filtering at the highest resolved wavenumbers, they observed that the vortex lines near the region of the maximum vorticity remain relatively straight during the late stages of growth, thus preventing the occurrence of blow-up in finite time. Bustamante & Kerr (2008), however, noted that there were 'ambiguities in the earlier description' of the initial conditions in Kerr (1993) which led to differences with the initial condition used by Hou & Li (2006). Bustamante & Kerr (2008) go on to explain these differences and to show evidence for a singularity with their initial conditions of two antiparallel vortices.

Orlandi & Carnevale (2007) instead considered the interaction of two colliding Lamb dipoles (Lamb 1932). Since these dipoles are form-preserving solutions of the Euler equations, there are no initial transients in their separate evolution. They simply propagate at constant speed. Since the velocity field of a dipole falls off as inverse distance squared in the direction perpendicular to the dipole axis, two dipoles can approach each other very closely before significant interaction begins. Thus, the two Lamb dipoles can be placed initially very close together, shortening the time before significant interaction takes place. Furthermore, no filtering appears to be necessary to avoid spurious regions of vorticity fluctuations outside the main cores in the initial

https://doi.org/10.1017/jfm.2011.430 Published online by Cambridge University Press

condition. The procedure for creating this initial condition is free of ambiguity since the vorticity distribution is based solely on the unperturbed Lamb dipole, the formula for which is well known (Lamb 1932; Batchelor 1967). Moreover, the Lamb dipole is an appropriate structure for detecting the approach of the energy spectrum toward the critical $n = -3$ power law because its initial spectrum is itself a power law behaving essentially as k^{-6} with some spectral oscillation. Orlandi & Carnevale (2007) have shown that this power law persists while the dipoles approach each other. Then, during the interaction, the spectrum preserves a power-law form, with the exponent increasing from $n = -6$ toward $n = -3$. This suggests the existence of a FTS, and the singularity time $t_s \approx 2.79$ can be estimated by extrapolation of the results as the $n = -3$ spectrum is approached. If the resolution is marginal, at a certain point there is an energy pile-up at high wavenumbers before the estimated t_s, but this does not affect the energy spectrum at large scales. If the inviscid simulations are allowed to evolve beyond t_s, then the spectrum tends to a k^2 energy equipartitioned spectrum at high k. This is a classic signature that the flow is not fully resolved. Cichowlas, Debbashn & Brachet (2006) have shown that the development of equipartitioning at high k, due to lack of resolution in an inviscid simulation, can act as a sink of energy for low k leading to the temporary formation of a $k^{-5/3}$ inertial range. This can be ascribed to the formation of unphysical vortical structures at high k. In time the equipartitioned k^2 spectrum extends down to the large scales. How to determine when an inviscid simulation is fully resolved is rather difficult quantitatively, but qualitatively it can be asserted that sufficient resolution is lost when an abrupt increase of energy is observed at high wavenumber. To show the effects of changing resolution on the achievement of the k^{-3} power law, we present here more refined simulations than those in Orlandi & Carnevale (2007). To better investigate the formation of the energy pile-up at the highest wavenumbers, we extend the simulations for a short period of time after the estimated inviscid t_s.

As noted above, evolution toward a k^{-3} power law is one of the indications of a FTS because if this power law were extended indefinitely in k, the enstrophy of the flow would be infinite. Of course, in a numerical simulation, necessarily with finite resolution, the full k^{-3} power-law spectrum could never be achieved. Furthermore, as the FTS is approached, the amplification of the enstrophy will require rapidly decreasing the computational time step, increasing the computational burden beyond practical limits. However, we hypothesize that the trend towards the FTS can be observed with the computational power currently available, and an extrapolation from well-resolved results can be made to estimate t_s. To search for evidence of the trend to a FTS, Orlandi & Carnevale (2007) analysed the vorticity components along the principal rate of strain axes, observing that the projection on the intermediate strain eigendirection ($\widetilde{\omega}_2$) is proportional to the corresponding eigenvalue ($\widetilde{S}_2$). This analysis suggests that the transport equation for $\widetilde{\omega}_2$ can be approximated by a model equation having a FTS. In this paper, more refined simulations, necessary to carefully analyse the time evolution of the energy spectra, reinforce our belief that the Euler equations have a FTS.

For the Navier–Stokes equations, the question is whether the viscous terms can prevent the formation of small regions with infinite velocity gradients given any finite viscosity ν, no matter how small. Alternatively, from the spectral point of view, we can ask whether the viscous terms will always result in the formation of a dissipation range at high wavenumber no matter how small ν. How this question can be answered numerically is a very difficult issue. If in a simulation a k^{-3} range were to form out to the maximum wavenumber k_{max}, the simulation would have to be repeated at

https://doi.org/10.1017/jfm.2011.430 Published online by Cambridge University Press

higher and higher resolution to show that, no matter how large k_{max}, no dissipation range will form. This program is certainly impractical given the physical limitations of computers. No matter how high we could make k_{max}, the result would always be subject to the criticism that it is not high enough. However, numerical simulations of the Navier–Stokes equations at high resolution can still provide insights that may help resolve the issue. Insight can be obtained by performing simulations at different Reynolds numbers and different resolution and observing the effect of these changes on the evolution of the enstrophy and on the evolution of each of the terms in the enstrophy evolution equation.

We investigate here the dynamics of vortex structures that can be related to various ranges of the energy spectrum in the dipole-collision problem. In viscous simulations of the collision, for relatively low R_λ, a short k^{-3} energy range develops. The spectrum also develops an exponential fall-off at high k indicating a dissipation range characteristic of turbulent flows. This dissipation range forms at a point in time much earlier than the estimated t_s from inviscid simulations, and the spectrum at high k is thus very different from the inviscid spectrum after that point. With increasing R_λ, the width of the k^{-3} range increases. The relation between the shape of the vortex structures in the flow and the exponent of the power law in the inertial range has been discussed by Orlandi (2009). Here we focus on the dynamics of these structures and analyse how they evolve. We will see, for example, how vortex sheets transform into vortex tubes. This transformation was studied in detail for vortex sheets in forced turbulence by Horiuti & Fujisawa (2008) at $R_\lambda \approx 75$. Their simulation resolved many vortex interactions occurring simultaneously in a domain large enough to capture them all. Consequently, they only had resolution sufficient to develop a short inertial range of about one decade in width. By focusing on just one event, we can better resolve the interaction and thus obtain a much wider inertial range.

In what follows, we discuss in detail the dynamics of the interacting vortices in inviscid and viscous flow. The numerical method and the initial conditions are presented in § 2. The inviscid analysis is given in § 3. Viscous results are presented in § 4. Finally, the inviscid and viscous results are compared in § 5.

2. Numerical method and initial conditions

The Navier–Stokes and the inviscid Euler equations are solved simultaneously with the continuity equation. Since the Euler equations are the same as the Navier–Stokes equations with $\nu = 0$, it is sufficient to present the Navier–Stokes equations. In dimensionless form, these are given by

$$\frac{\partial u_i}{\partial t} + \frac{\partial u_i u_j}{\partial x_j} = -\frac{\partial p}{\partial x_i} + \frac{1}{Re}\frac{\partial^2 u_i}{\partial x_j^2}; \quad \frac{\partial u_i}{\partial x_i} = 0, \tag{2.1}$$

where p is the dimensionless pressure. The Einstein summation convention on repeated indices is used throughout this paper, and also assumed for quadratic indexed variables (e.g. $u_i^2 \equiv u_i u_i \equiv \sum_i u_i^2$) except where specified otherwise. For the viscous simulations of colliding Lamb dipoles, the Reynolds number is defined as $Re = Ua/\nu$, with U the propagation velocity and a the radius of the dipoles. In polar coordinates centred on the dipole, the vorticity distribution is

$$\begin{aligned} \omega &= -2U\kappa \frac{J_1(\kappa r)}{J_0(\kappa a)} \sin(\theta - \theta_0), \quad (r < a), \\ &= 0 \quad (r > a), \end{aligned} \tag{2.2}$$

https://doi.org/10.1017/jfm.2011.430 Published online by Cambridge University Press

where κ is a constant and $\kappa a = j_1^1 \approx 3.8317$ is the first strictly positive zero of the Bessel function J_1. Equation (2.2) is a steady solution of the Euler equations in the co-moving reference frame. The dipole propagates in the direction $\theta = \theta_0$, and it can be located at any position in the computational box by changing the point of origin of the radius r.

One may criticize the use of the Lamb dipole for present purposes because the radial derivative of the vorticity is not continuous at $r = a$. However, at $r = a$ the vorticity is zero, and this boundary does not play a role in the amplification of vorticity (Orlandi & Carnevale 2007).

The initial 3D vorticity distribution of two colliding dipoles is constructed by assigning the vorticity distribution given by (2.2) on the x_1–x_2 plane, centred at $x_1 = \pi/2$ and $x_2 = 0$, and extending vorticity component ω_3 uniformly in the x_3 direction. The orientation of this dipole is such that it moves in the negative x_1 direction. The second dipole with vorticity ω_2 along x_2, is centred at $x_1 = -\pi/2$ and $x_3 = 0$. Its vorticity is extended uniformly in the x_2 direction, and it moves in the positive x_1 direction.

In the inviscid simulations, as described by Orlandi & Carnevale (2007), the equations are solved in a cubic box of size 2π with the periodicity assumption in the three directions. To save computational time, symmetries are imposed with respect to two coordinate planes, so that only one quarter of the full domain is actually simulated. The size of this domain proved adequate because the estimated singularity time t_s was found to occur before any parts of the colliding dipoles traversed the width of the domain. However, in the viscous case the simulations can evolve for a longer time, and parts of the dipole distant from the interaction region continue to travel covering the distance 2π. Therefore, it is found to be necessary to run such long simulations in a domain extended in the x_1 direction.

The present simulations were performed with a second-order finite-difference scheme, with staggered velocities. This scheme is energy conserving in the limit of $\Delta t \to 0$. Orlandi (2000) validated this scheme for inviscid and viscous simulations. It has been demonstrated that this scheme can achieve results matching those of pseudospectral methods in simulations of the Taylor–Green flow (Duponcheel, Orlandi & Winckelmans 2008). Orlandi (2009) presented a comparison between the energy spectra in forced isotropic turbulence obtained by the present numerical method and those obtained by pseudospectral methods in Jimenez *et al.* (1993) and Gotoh, Fukayama & Nakano (2002). Owing to differences in the forcing used in the two studies, the results differed at low wavenumber. On the other hand the agreement was good at $\eta k \approx 1$ (η is the Kolmogorov length scale). The interesting outcome of the comparison was that the second-order finite-difference energy-conserving scheme produces less energy pile-up at the spectral truncation wavenumber k_{max} than does the pseudospectral scheme. The energy-conserving finite-difference scheme should then be appropriate to deal with inviscid flows which ideally should lead to a k^{-3} power law in the entire range in the event of a FTS.

3. Results: Euler

3.1. *Energy spectra*

As noted above, there is still no convincing theoretical proof as to the existence of a FTS for the Euler equations given smooth initial conditions. Although there is no way to actually prove (or disprove) the existence of a FTS numerically, DNSs can give insights that can be and have been very helpful to theoreticians considering this

https://doi.org/10.1017/jfm.2011.430 Published online by Cambridge University Press

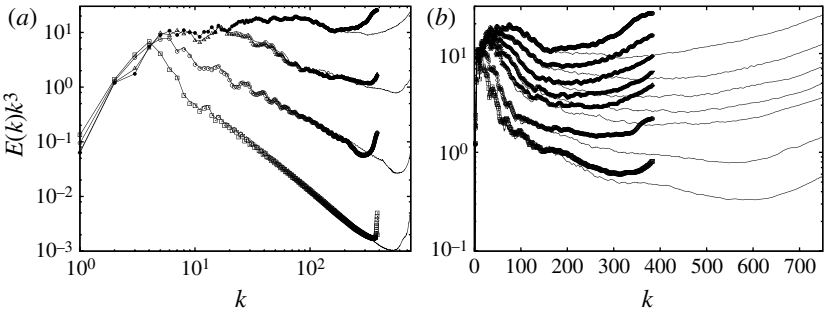


FIGURE 1. Compensated energy spectra for the colliding Lamb dipoles. (*a*) the spectra at $t = 1.5$ (□), $t = 2.0$ (○), $t = 2.5$ (△), $t = 2.73$ (●) resolution 768^3; lines resolution 1536^3. (*b*) The spectra at times closely approaching t_s: $t = 2.5, 2.58, 2.65, 2.67, 2.69, 2.71$ and $t = 2.73$ from bottom to top, symbols 768^3, lines 1536^3.

problem. This was emphasized by Majda & Bertozzi (2002, Chapter 5) in their call for simulations at higher resolution. They noted that the influential simulations by Kerr (1993) and Brachet *et al.* (1983) were obtained with computers that were rather inefficient compared to those available today. As discussed in the introduction, Kerr (1993) examined the evolution of a perturbed pair vortices with a Gaussian vorticity distribution searching for evidence of a FTS. Brachet *et al.* (1983), on the other hand, considered the Taylor–Green flow. The velocity distribution for the Taylor–Green flow can be found in that article or in Cichowlas & Brachet (2005), which also provides a study of the evolution of the Taylor–Green flow with different numerical resolutions.

Orlandi (2009) found that during the collision of Lamb dipoles the energy spectra roughly maintains power-law behaviour in which the spectrum becomes shallower with time. At $t = 0$ the spectrum for the dipoles has a wide k^{-6} power law. As the two dipoles come into contact and begin to deform, the exponent of the power law n becomes less negative. Figure 1(*a*) shows that at $t = 1.5$ it reduces to $n = -4.7$, and it reaches the value $n \approx -3$ at a time approximating the estimated inviscid t_s. Note that the $n = -3$ range first forms in the energy containing scales. Although any finite resolution grid will not be sufficient to prove the existence of an infinite $n = -3$ range, the evidence based on the comparison between spectra from the 768^3 and 1536^3 grid simulations suggests the existence of an infinitely extended k^{-3} power law for infinite resolution. A more detailed view of the spectra at times near t_s is given in figure 1(*b*) where the k-axis is linear.

The compensated spectra $k^3E(k)$ in figure 1 emphasize the effects of small scales. To give a better idea of how well our simulations are resolved, and to permit ready comparison with previous work such as the study of Hou & Li (2006) based on the Kerr (1993) initial condition of antiparallel vortices, we also display the evolution of the energy and enstrophy spectra for various resolutions in figure 2. Over the corresponding domains of validity, all of these spectra are in agreement. Up until $t = 2.7$, the resolution is excellent with energy falling off by at least seven orders of magnitude and the enstrophy by more than two orders of magnitude in the highest-resolution runs. As the estimated singularity time is approached, the spectra do rise rapidly, but this is to be expected if approaching the singularity is associated with producing a k^{-3} energy spectrum. Figure 2(*c*) shows that the spectra nearly match a k^{-3} fall-off over a region that becomes longer the higher the resolution. The comparison between the spectra of different resolutions suggests that the approach to

https://doi.org/10.1017/jfm.2011.430 Published online by Cambridge University Press

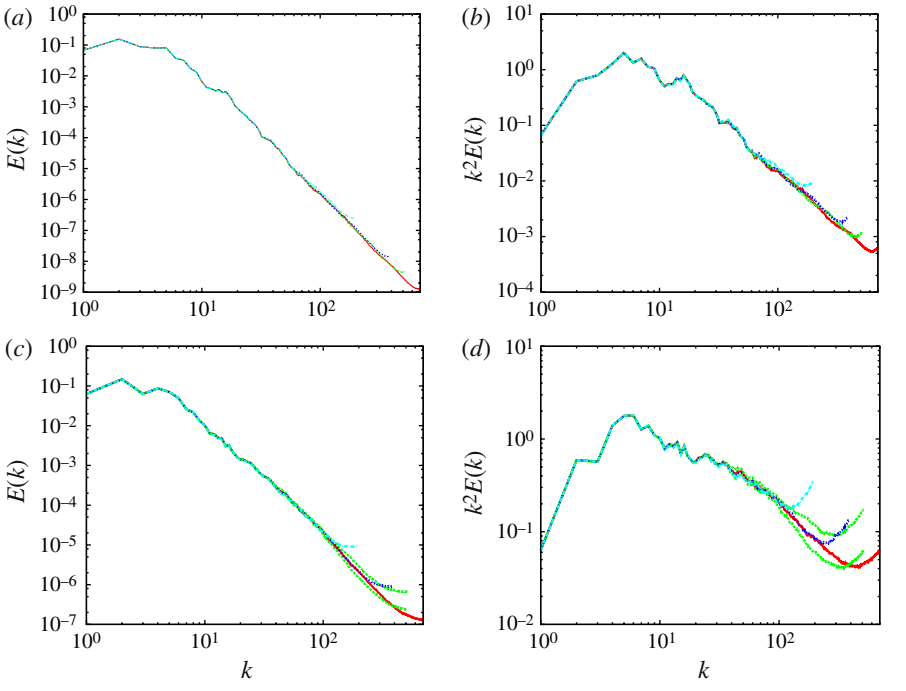


FIGURE 2. (Colour online available at journals.cambridge.org/flm) Energy spectra (*a*,*c*,*e*) and enstrophy spectra (*b*,*d*,*f*) at (*a*,*b* $t = 2.50$; (*c*,*d*) at $t = 2.75$ for different resolutions: red 1536^3, green 1024^3, dark blue 786^3 and light blue 384^3. In (*c*) and (*d*) for 1024^3, instead of one spectrum at $t = 2.75$, we show two spectra, one at $t = 2.74$ and the other at $t = 2.76$, to show how rapidly the spectrum changes during this period.

a k^{-3} energy spectrum will continue as higher resolution becomes possible. On the other hand, the curling up of the energy and enstrophy spectra at the high-wavenumber end is related to lack of resolution. By $t = 2.75$, this curl up appears significant, particularly in the enstrophy spectrum (figure 2*d*). In figures 2(*c*,*d*), there are actually two curves (green) corresponding to resolution 1024^3. Instead of $t = 2.75$ these two curves represent the state at $t = 2.74$ and $t = 2.76$. These two panels illustrate how rapidly the ends of the spectra are curling up at $t = 2.75$.

The three-dimensional structure of the colliding dipoles and the positions of the vortex structures where the amplification is taking place was shown by Orlandi & Carnevale (2007) (figure 11) for the case of a resolution 1024^3. Additionally, in their figure 15, they showed the contour plot of $|\omega|$ in the $x_1 = 0$ dividing plane where the dipoles collide. Here we again plot $|\omega|$ in the $x_1 = 0$ plane, but now for the higher-resolution case of 1536^3. To enhance visualization of the high $|\omega|$ levels we actually plot $\log(|\omega|)$. By symmetry, the $|\omega|$ field will look the same in each of the four quadrants of the $x_1 = 0$ plane. In figure 3 we show only the fourth quadrant, and of that only the region $(-2.2 \leqslant x_2, x_3 \leqslant -1.1)$ in which significant amplification takes place. Figure 3(*a*) shows that at $t = 2.65$ there are two points where $|\omega|$ is maximum, one in each of the two ovals in the lower left portion of the plot. These ovals are cross-sections of long tube-like structures in the 3D domain (see Orlandi & Carnevale 2007). At $t = 2.7$, the maxima of $|\omega|$ are in the very thin curved red arcs in the structure in the upper right part of the domain. These curved arcs are cross-sections of

https://doi.org/10.1017/jfm.2011.430 Published online by Cambridge University Press

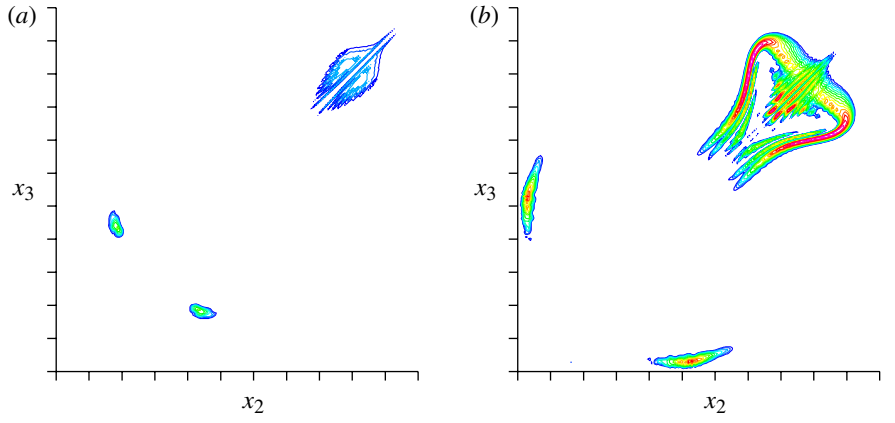


FIGURE 3. (Colour online) Two-dimensional contour plots of $\log(|\omega|)$ at (*a*) $t = 2.65$ and (*b*) at $t = 2.70$, at 1536^3 resolution, with contour interval $\Delta = 0.05$, starting from $\log(|\omega|) = 5.277$ (for *a*), 5.667 (for *b*) ($-2.1 \leqslant x_2, x_3 \leqslant -1.3$).

sheet-like structures in the 3D field. One maximum occurs in each of the two red arcs, approximately at the point of greatest curvature. Orlandi & Carnevale (2007) showed that within these arcs of high vorticity the strain rate is aligned with the vorticity and that this leads to the rapid amplification of vorticity. While this is happening, these curved vorticity sheets continue to thin and bend.

3.2. *Enstrophy evolution*

The tendency toward a k^{-3} power law is one possible indication of the existence of a FTS for either the Euler equations or the Navier–Stokes equations. Several other indicators have been discussed by Kerr (2006) and by Galaktionov (2009), and some of them were demonstrated by Orlandi & Carnevale (2007). Pumir & Siggia (1990) suggest a singularity with velocity increasing at least as rapidly as $(t_s - t)^{-1/2}$ and vorticity diverging at least as fast as $(t_s - t)^{-1}$ at singularity time t_s. Furthermore, the theorem of Beale, Kato & Majda (1984) for the Euler equations implies that if there is a singularity with the maximum of the magnitude of the vorticity growing as $(t_s - t)^{-n}$ then $n \geqslant 1$ (Gibbon 2008).

Given these results and suggestions, it would be interesting investigate whether in inviscid simulations there may be an indication of a FTS with the magnitude of velocity increasing as $(t_s - t)^{-1/2}$, length scales decreasing as $(t_s - t)^{1/2}$ and magnitude of vorticity increasing as $(t_s - t)^{-1}$. The global conservation of energy implies that if there is a region where the velocity is growing as $(t_s - t)^{-1/2}$, then this area must be shrinking in volume. A precise measurement of the reduction rate of the volume where the energy density is growing is difficult. Flow visualizations, in the period of strong vorticity amplification, showed that this is a thin sheet reducing its thickness and width proportionally to $(t_s - t)^{1/2}$ (Orlandi & Carnevale 2007). The formation of structures of this kind agrees with the observation that in turbulent flows ribbon-like structures are driving the energy cascade within the inertial range (Orlandi 2009).

Estimating t_s and γ from data for some quantity $f(t)$ that hypothetically has a FTS and behaves as

$$f(t) = C\,(t_s - t)^{-\gamma}, \tag{3.1}$$

https://doi.org/10.1017/jfm.2011.430 Published online by Cambridge University Press

near t_s, in practice proves to be a difficult problem. In addition to matching the three parameters C, t_s and γ to the data, one must also chose the appropriate region of time over which to make the fit. The scaling behaviour in a simulation is only over some limited period of time, say from $t = t_i$ to $t = t_f$. The choice of t_i and t_f plays an important role on the determination of the values of C, t_s and γ. Bustamante & Kerr (2008) suggested that it is useful to examine the logarithmic derivative of $f(t)$ instead of $f(t)$ directly since this eliminates the need to estimate the constant C in estimating t_s and γ. Here we apply this idea to the enstrophy of the flow. The enstrophy evolution equation, with $\Omega = \langle \omega_i^2 \rangle / 2$, where $\langle \ldots \rangle$ indicates a volume integral over the entire domain, can be written in terms of the logarithmic derivative of Ω:

$$\frac{1}{\Omega}\frac{\mathrm{d}\Omega}{\mathrm{d}t} = \frac{P_\Omega}{\Omega}, \tag{3.2}$$

where $P_\Omega = \langle \omega_i \omega_j S_{ij} \rangle$ is the enstrophy production and $S_{ij} \equiv \frac{1}{2}(\partial_i u_j + \partial_j u_i)$ is the rate of strain tensor. If $\Omega \approx C\,(t_s - t)^{-\gamma}$ for any value of γ, the left-hand side of (3.2) is proportional to $(t_s - t)^{-1}$. In practice, the data will approximate this behaviour only for a limited period, (t_i, t_f). The time t_i, when strong amplification of Ω begins, depends on the initial conditions of the flow; t_f is the time when strong amplification ceases due to lack of resolution, and is very resolution dependent, but should increase systematically with higher resolution. An important requirement is that $t_f - t_i$ should be relatively long. If the dimensionless quantities $\tau = (t - t_i)/(t_s - t_i)$ and $Q(0)/Q(\tau)$, where $Q(\tau) \equiv P_\Omega / \Omega$, are introduced, and if the FTS does exist, then $Q(0)/Q(\tau)$ should fit the line $1 - \tau$ only if the estimated t_s is the real time of the FTS. Note that by focusing on the ratio $Q(0)/Q(\tau)$, we can determine t_s independently of γ. Since t_s cannot be exactly determined, for the lack of resolution, it must be evaluated by an extrapolation of the results obtained by the fully resolved simulations in the period of time before the development of unphysical small scales as discussed above. For example, in figure 4(*a*) we show the result of setting $t_i = 2.6$ and using two tentative values for t_s ($t_1 = 2.75$, $t_2 = 2.815$) to draw the data. The graphs are then fit by the thin lines shown. These lines intersect the $Q(\tau) = 0$ axis at $\tau_1 = 1.25$, $\tau_2 = 0.85$. Using linear interpolation between these two values to obtain $Q(\tau) = 0$ for $\tau = 1$ yields $t_s = 2.79$. At this stage it is not clear whether our simulations underestimate or overestimate the 'true' singularity time. Straightforward linear least-squares fitting of the Q data yields very similar values. The values of t_i and t_s thus determined will be hereafter used for presentation purposes.

Having estimated t_s, from P_Ω / Ω, it is now important to see whether $|u_i^2|_\infty$ and $|\omega_i|_\infty$ behave as $(t_s - t)^{-1}$.

Figure 4(*b*) shows that $|u_2|_\infty^2$ follows the expected linear behaviour fairly well during the period of strong vorticity amplification. The results are plotted for two resolutions: 1024^3 and 1536^3. In the higher-resolution simulation the results follow the expected trend for a longer time than in the coarser simulation. Note that in the resolution 1536^3 case, the data bend away from the singularity scaling around $\tau = 0.8$, while for the case with resolution 1024^3, the data bend away from the linear scaling line and flatten out earlier, at approximately $\tau = 0.7$. Thus, the t_f discussed above does increase with resolution as would be expected if increasing resolution actually does bring the flow closer to singularity. By symmetry $|u_2|_\infty = |u_3|_\infty$, and the component u_1 is mainly related to the translation velocity of the two dipoles, which is constant while the two dipoles approach each other, and so does not increase while the dipoles interact. Therefore, $|u_3|_\infty$ and $|u_1|_\infty$ have not been plotted.

https://doi.org/10.1017/jfm.2011.430 Published online by Cambridge University Press

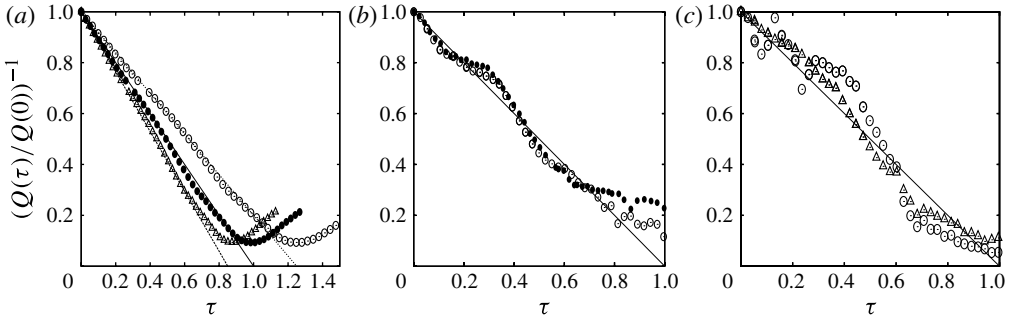


FIGURE 4. (*a*) Diagram used to evaluate t_s from $Q = P_\Omega/\Omega$ as a function of $\tau = (t - t_i)/(t_s - t_i)$ with $t_i = 2.6$ for the simulation with resolution 1536^3. The open circles and triangles are the data $Q(\tau)$ as evaluated for t_1 and t_2 as explained in the text. The filled circles are for $Q(\tau)$ evaluated with the calculated t_s. (*b*) $Q = |u_2|_\infty^{-2}$ for the colliding-dipoles flow (○, resolution 1536^3), (●, resolution 1024^3); (*c*) $Q = |\omega|_\infty^{-1}$ (○) and $Q = |\widetilde{\omega}_2|_\infty^{-1}$ (△) (resolution 1536^3). (τ is defined with $t_s = 2.79$ and $t_i = 2.6$.)

Regarding the growth of $|\omega|_\infty$ for the colliding dipoles, Orlandi & Carnevale (2007) observed that it behaves like $|\widetilde{\omega}_2|_\infty$, and that both of these quantities agreed satisfactorily with the expected $(t_s - t)^{-1}$ scaling for simulations with resolution (1024^3). Figure 4(*c*) shows that the new data for $|\omega|_\infty^{-1}$ and $|\widetilde{\omega}_2|_\infty^{-1}$ from the (1536^3) simulation agree rather well with the $(t_s - t)$ scaling, even though there is some oscillation around the linear scaling law.

We have shown that the period of singular scaling increases with resolution in the case of $|u_2|_\infty$. Next we present a resolution study of the behaviour of $|\omega|_\infty$. Figure 5(*a*) shows the behaviour of $|\omega|_\infty^{-1}$ on the interval $[t_i, t_s]$ for simulations of four different resolutions. Although there is some evidence that the scaling behaviour is better the higher the resolution, there is also significant oscillation around the straight line scaling. Hou & Li (2006) suggest plotting the hypothetical constant $C = (t_s - t)|\omega|_\infty$. This is done in figure 5(*b*) from $t_i = 2.6$ to $t_s = 2.79$. In Hou & Li (2006, figure 9), the value of C gradually increases and then falls off near t_s. Our graph of C is somewhat noisier, but does display a flat period up to $\tau = 0.6$ ($t \approx 2.7$), then increases rapidly before falling off due, we believe, to insufficient resolution. The falloff occurs after about $\tau = 0.8$ ($t = 2.75$) in agreement with our estimate of when resolution effects would become significant based on spectral considerations. As explained in Orlandi & Carnevale (2007), the most interesting vorticity component to analyse is $|\widetilde{\omega}_2|_\infty$, the component aligned along the direction corresponding to the eigenvector of intermediate eigenvalue of the rate of strain tensor. In figure 5(*c*), we see that the values of $|\widetilde{\omega}_2|_\infty$ do follow the straight-line scaling better than the values of $|\omega|_\infty$, and the results improve with increasing resolution. Note that t_f, the time where the data leave the line due to insufficient resolution, increases with resolution. The evolution of the hypothetical constant C is also somewhat more convincing when calculated from $|\widetilde{\omega}_2|_\infty$ as seen in figure 5(*d*).

Orlandi & Carnevale (2007) argue that the rapid growth of $|\widetilde{\omega}_2|_\infty$ is related to the rapid growth in the intermediate eigenvalue $\tilde{S}_2$ of the rate of strain tensor. They performed a resolution check showing that this is the case for various resolutions from 480^3 to 1024^3. Rapid growth in $\tilde{S}_2$ does continue even as the resolution is increased. In figure 6(*a*), the evolution of $\tilde{S}_2$ is shown for the new higher resolution 1536^3, as well as for resolutions 768^3 and 1024^3 for comparison. Although the data are noisy, and

https://doi.org/10.1017/jfm.2011.430 Published online by Cambridge University Press

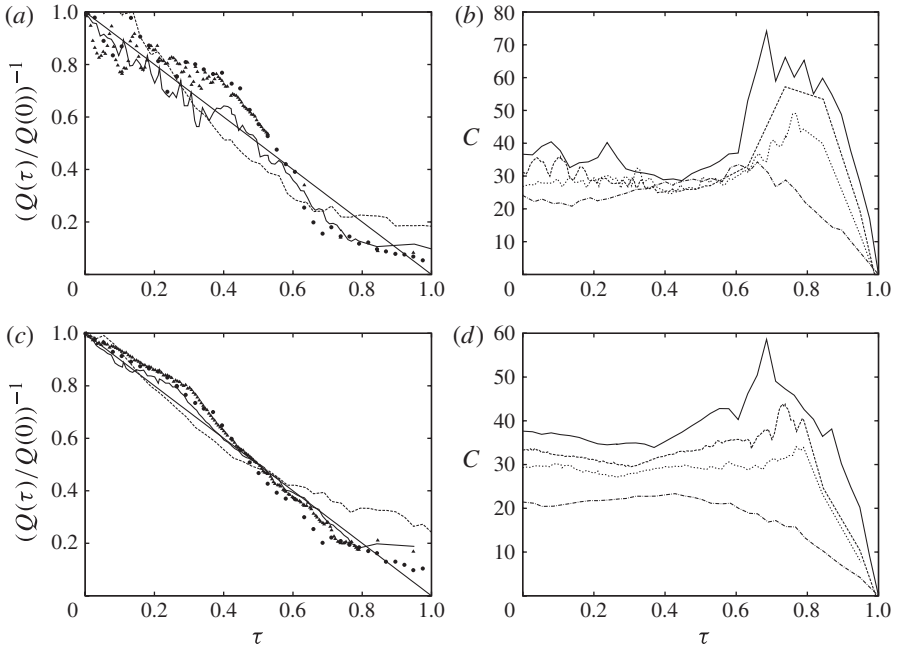


FIGURE 5. During the period of rapid amplification for the colliding dipoles, we show the evolution of: (*a*) $Q = |\omega|_\infty^{-1}$ and (*c*) $Q = |\widetilde{\omega}_2|_\infty^{-1}$ (○, resolution 1536^3), (▲, 1024^3, thin solid line (768^3), thin dashed line (384^3). (*b*) $C = (t_s - t)|\omega|_\infty$ and (*d*) $C = (t_s - t)|\widetilde{\omega}_2|_\infty$, shown for resolutions 1536^3, 1024^3, 768^3 and 384^3 (the darker the curve, the higher the resolution). The time-like variable $\tau = (t - t_i)/(t_s - t_i)$ is defined with $t_s = 2.79$ and $t_i = 2.6$.

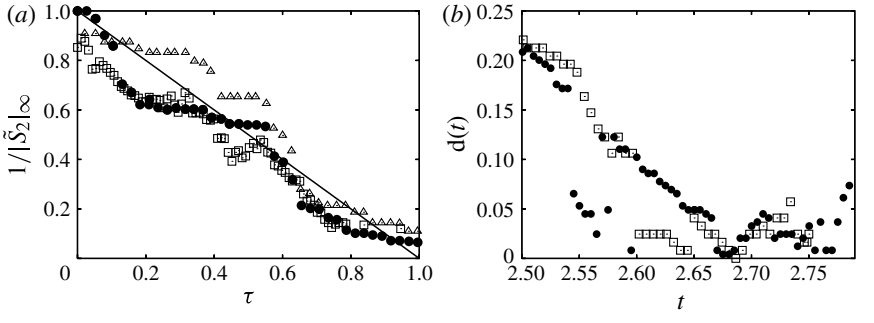


FIGURE 6. (*a*) $\tilde{S}_2$ for resolutions 1536^3 (○), 1024^3 (□) and 768^3 (△). (*b*) The distance from the plane $x_1 = 0$ to the point where $|\omega|$ is maximal for resolutions 1536^3 (○) and 768^3 (□).

there is flattening of the signal (after about $\tau = 0.8$ for the highest resolution case), the data do roughly follow the linear scaling line.

Another interesting diagnostic is the distance of the point of maximum $|\omega|$ from the $x_1 = 0$ plane. For the period from $t = 2.5$ to $t = 2.65$ the data in figure 6(*b*) show two sequences of data with d(t) decreases linearly with time representing a speed of approach of ∼1. These represent competing maxima in different intense vortex structures. After this the distance is subject to noise with fluctuations up to ∼0.07 units. It seems that the maxima are contained in regions of high $|\omega|$ extending roughly

https://doi.org/10.1017/jfm.2011.430 Published online by Cambridge University Press

0.07 units out from the $x_1 = 0$ plane. This distance represents $\sim$17 grid points at resolution 1536^3. Perhaps the true point of maximum $|\omega|$ could be approximated better within these regions with some interpolation, but this has not been done here where the data is examined only on the computational grid.

The energy is well conserved in these simulations almost up to the estimated singularity time t_s. In the highest-resolution case, the energy was conserved at least up to five significant figures until $t = 2.74$. Even if we go to the predicted singularity time, the relative error in the energy is still less than 0.03 %. The energy would be even better conserved if a smaller time step were used since the scheme is conservative in the limit $\Delta t \to 0$. Here we are using a fixed Courant–Friedrichs–Lewy number $\mathrm{CFL} \equiv u_{max}\Delta t/\Delta x$, where Δx is the mesh size, constant in all three grid directions in our case. By comparing results at resolution 384^2, we found that there was not much difference using $\mathrm{CFL} = 0.5$ compared with $\mathrm{CFL} = 1.5$ in this simulation, but the errors with $\mathrm{CFL} = 2.25$ are unacceptable. We have used $\mathrm{CFL} = 0.5$ in the results reported here. As the singularity time, t_s is approached, the time step decreases, but apparently not rapidly enough to preserve energy conservation near t_s. Making CFL much smaller would allow energy conservation up to times closer to t_s, but due to limited computational resources, this is impractical. Note that for any finite resolution, the singularity must be killed as t_s is approached, no matter how small we make Δt. Once the amplifying vortex structures become unresolved, amplification will cease. Thus, it makes more sense to put computational resources into reducing the mesh size rather than reducing CFL further.

From flow visualizations we observed that ω_i^2/Ω grows in a region which shrinks in time. To examine this quantitatively, we calculated the volume of regions where ω_i^2/Ω is greater than an *a priori* threshold value O_T. Lack of resolution results in intense scattered vorticity noise that makes spectral filtering desirable for volume rendering of the velocity and vorticity fields. However, since we are looking for evidence of a rapidly shrinking volume, spectral truncation will in part smooth out just the structures in which we are most interested. This is an unavoidable problem since there is no easy way to separate the noise from the signal. Filtering is accomplished by setting equal to zero all Fourier amplitudes with wavenumber greater then some k_{trunc}. We can get a quantitative idea of the effect of this truncation by looking at the effect that truncating with various k_{trunc} has on the probability density functions (p.d.f.s) for ω_i^2/Ω. Figure 1(*b*) may suggest we start with a $k_{trunc} = 400$ since it is about at this k that the compensated spectrum begins to slope up, particularly as $t \to t_s$, presumably indicating unphysical growth of energy in high wavenumbers due to inadequate resolution. In figure 7(*a*) we show the p.d.f.s of $X = \omega_i^2/\Omega$ for the period for $2.60 \leqslant t \leqslant 2.75$ for both the unfiltered vorticity and for the vorticity filtered with $k_{trunc} = 400$ for the simulation of resolution 1536^3, that is with $k_{max} = 768$. The p.d.f.s for the unfiltered (filtered) vorticity are shown as solid (dashed) curves draw at times separated by $\Delta t = 0.05$. Filtered or unfiltered, we see that the number of locations with very intense $|\omega|$ increases as t approaches t_s. We have also considered $k_{max} = 600$ and the results are very similar to those for $k_{max} = 400$. The unfiltered and filtered p.d.f.s do not differ much for low values of X, but they do at the extremely high values especially at $t = 2.75$. Clearly at $t = 2.75$ the filtering significantly eliminates vorticity generated by the insufficient resolution, but perhaps also in part generated by the amplification of ω expected for the approach to a FTS. The p.d.f.s for $k_{trunc} = 400$ and $k_{trunc} = 600$ do not differ much, but for better flow visualizations introduced later, the most useful results are obtained with $k_{trunc} = 400$. The changing p.d.f. shows that as t_s is approached, the proportion of sites where X takes on its highest values is

https://doi.org/10.1017/jfm.2011.430 Published online by Cambridge University Press

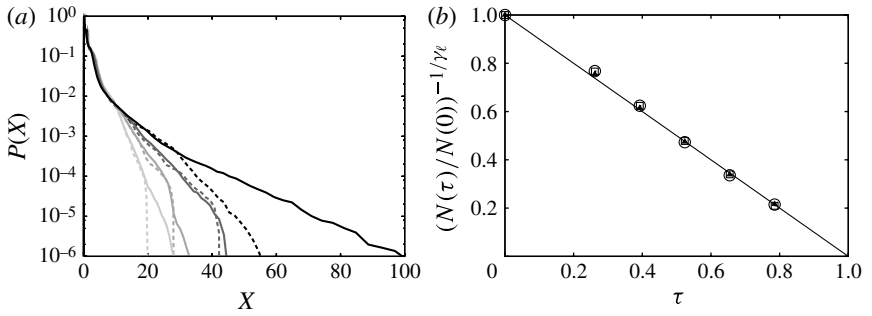


FIGURE 7. (*a*) The p.d.f. of $X = \omega_i^2/(\Omega/2)$ for colliding dipoles (resolution 1536^3) at times from $t = 2.6$ to $t = 2.75$ in increments $\Delta t = 0.05$ with no truncation (solid curves) and with $k_{trunc} = 400$ (dashed). The increasing darkness of the curves corresponds to increasing time. (*b*) Number of points (referred to time $t_i = 2.6$) where $X > X_T$ for $X_T = 7$ (○), $X_T = 10$ (△) and $X_T = 15$ (□).

decreasing relative to the total volume. The p.d.f. tends toward a distribution, at late times, with long tails.

Next we calculated a measure of the reduction in the number of points with high X using different values of the threshold O_T. If the threshold value is low then it is uninteresting because we are including regions without strong amplification. On the other hand, if O_T is too high, no regions will be found early in the period of amplification, making it difficult to define the trend in time. As a compromise, we show the results for three choices of O_T: 7, 10 and 15 in figure 7(*b*). The number of points for which $\omega_i^2/\Omega > O_T$ for each of these three choices is N_l, with $l = 1, 2, 3$, corresponding to the three choices of O_T in increasing order. For each l we find $N_l(\tau)/N_l(0) \approx (1-\tau)^{-\gamma_\ell}$. The values of γ_ℓ have been calculated by a best fit, obtaining for the three O_T respectively $\gamma_\ell = -0.27$, -0.33 and -0.38. The result is plotted in figure 7(*b*) where we note that there is very little scatter in the data.

Taking into account these ideas about the shrinking volume in which we find increasing extreme levels of vorticity, we understand that the growth of Ω ($\Omega \approx (t_s - t)^{-\gamma}$), a global integral quantity ($\Omega = \int \omega^2 \, \mathrm{d}V$) cannot grow as fast as $|\omega|_\infty^2$. The relative contributions that regions with different values of ω_i^2 make to the total enstrophy can be estimated through the p.d.f.s in figure 7(*a*). Such an analysis suggests that Ω should approach the singularity at t_s with a smaller exponent γ than that for $|\omega|_\infty^2$. The trend for Ω is given in figure 8(*a*). This figure shows a weak dependence on resolution, and we see once more that the fit to our proposed linear scaling relation gets better with increasing resolution. This is consistent with our hypothesis that the deviation is caused by lack of resolution and not to a physical mechanism that is limiting the singularity. The linear relation defined here has $\gamma = 3/4$. If $\Omega \approx (t_s - t)^{-3/4}$, then from the enstrophy equation, P_Ω should be $P_\Omega \approx (t_s - t)^{-7/4}$. This is confirmed by the numerical simulations as can be seen in figure 8(*b*). Note that the data in figure 8 are plotted using the same values of t_i and t_s as used in figure 4. These figures show that $\Omega^{-4/3}$ and $P_\Omega^{-4/7}$ fit the linear trend $1 - \tau$ very well.

Lu & Doering (2008) investigated states of maximal enstrophy production for the Navier–Stokes equations using a variational approach. They found two branches of solutions obeying the relation $P_\Omega = C\Omega^\alpha$ for the Navier–Stokes equations: a high-energy branch with $\alpha = 3$ and a low-energy branch with $\alpha = 1.78$. In our inviscid simulation, we find different relations between Ω and P_Ω depending on what phase

https://doi.org/10.1017/jfm.2011.430 Published online by Cambridge University Press

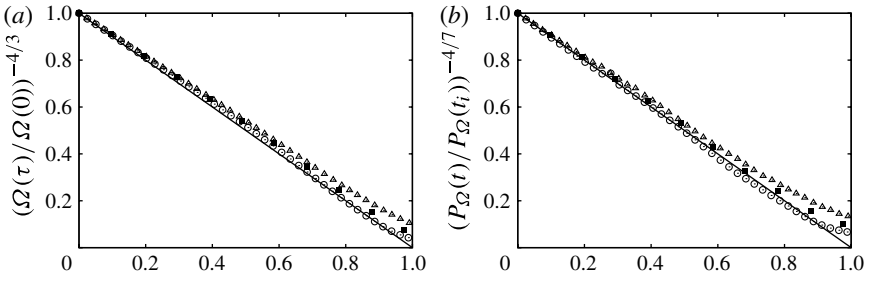


FIGURE 8. $\Omega^{-4/3}$ and $P_\Omega^{-4/7}$ versus τ during the period of rapid amplification. (*a*) $\Omega^{-4/3}$ and (*b*) $P_\Omega^{-4/7}$ for simulations of different resolutions (768^3, △; 1024^3, ■; 1536^3, ○).

of the evolution is examined. Before the collision, $P_\Omega \approx 0$ (i.e. there is no vortex stretching). When the dipoles begin to deform each other, there is a period in which Ω and P_Ω grow exponentially with $P_\Omega \propto \Omega$. In the period of rapid vorticity amplification before t_s, we find $P_\Omega \approx \Omega^{7/3}$, i.e. $\alpha \approx 2.33$, which is larger than the lower branch result of Lu & Doering (2008). In the next section, we examine α for the viscous colliding dipole.

The exponent of the inverse power-law trend of the enstrophy toward the possible FTS is also related to the self-similar nature of the singularity. As shown by Constantin (1994), globally self-similar blow-up of the Euler equations requires that length scales collapse in all directions as $L \sim (t_s - t)^{2/5}$. Hence, assuming that $\omega_\infty \sim (t_s - t)^{-1}$, it follows that $\Omega \sim \omega_\infty^2 L^3 \sim (t_s - t)^{-4/5}$. Of course, in the case that self-similarity is not complete, the exponent should be less than 4/5 in absolute value. Our result that $\Omega \sim (t_s - t)^{-3/4}$ (even though the singularity exponent is not too far from maximal) implies lack of full 'global' self-similarity, and in this sense, the possible FTS should be 'local'. This result has never been noticed before, and it may contribute to the singularity debate.

Further information on the nature of the possible FTS can be gained by checking the validity of theoretical estimates related to the growth of the maximum vorticity and of the vortex stretching term. Hou & Li (2006) examined the possibility that $|\omega|_\infty$ grows no faster than a double exponential in time. For their simulation of antiparallel vortices, they found that $\log\log|\omega|_\infty$ is almost linear but with negative curvature, hence the growth is at most double exponential, indicating no singularity. In figure 9(*a*), we plot $\log\log|\omega|_\infty$ for the colliding Lamb dipole simulations with two different resolutions. For this initial condition, the graphs are not linear and the curvature is overall positive. The figure also shows a direct comparison with our results for $\log\log|\omega|_\infty$ and the curve $\log\log(\theta/(t_s - t))$, where θ is a constant adjusted to match our data at $t_i = 2.6$. This shows that our data does match this growth fairly well at least up to $t \approx 2.74$, after which finite resolution effects may be reasonably considered to be forestalling the acceleration of the growth. This is rather different from the case shown in Hou & Li (2006, 2008) for their simulations based on the evolution of a pair of antiparallel vortices.

Another important diagnostic to check is the vortex stretching factor α (Constantin 1994) defined by

$$\alpha \equiv \frac{\omega_i S_{ij} \omega_j}{|\omega|^2}. \tag{3.3}$$

https://doi.org/10.1017/jfm.2011.430 Published online by Cambridge University Press

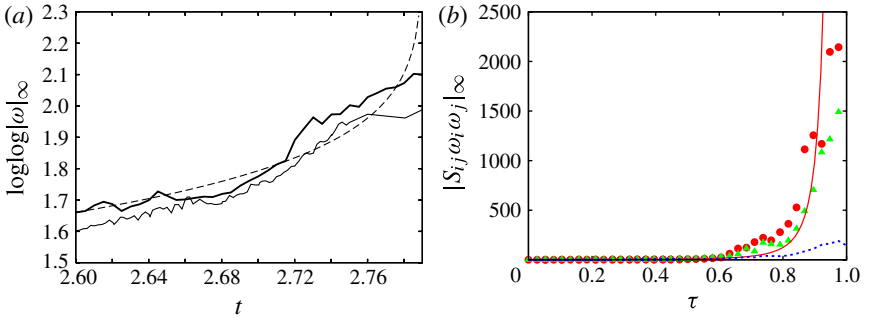


FIGURE 9. (Colour online) (*a*) $\log\log|\omega|_\infty$ with resolution 768^3 (thin line), resolution 1536^3 (thick line) and the theoretical blow-up curve $\log\log(\theta/(t_s - t))$ (dashed line); (*b*) $|S_{ij}\omega_i\omega_j|_\infty$ (●), the blow-up estimate ($|\omega|_\infty^3$) (▲), the theoretical blow-up curve $(t_s - t)^{-3}$ (solid line), and Hou & Li's non-blow-up estimate ($|\omega|_\infty^2 \log|\omega|_\infty$) (dotted line), all from the 1536^3 simulation.

The growth of the magnitude of the vorticity is given by $D_t|\omega| = \alpha|\omega|$, so it would be natural to examine the value of α where $|\omega|$ is maximal. However, measuring the quantity α evaluated at this point is subject to large discretization errors (see Pumir & Siggia 1990). An alternative is to consider

$$\hat{\alpha} \equiv \frac{|\omega_i S_{ij}\omega_j|_\infty}{|\omega|_\infty^2}, \tag{3.4}$$

as was done by Pumir & Siggia (1990). For colliding Lamb dipoles at resolution 1024^3, Orlandi & Carnevale (2007) presented and compared both α at the point of maximum $|\omega|$ and $\hat{\alpha}$. As anticipated by Pumir & Siggia (1990), the α data were very noisy, while the $\hat{\alpha}$ data proved sufficiently clean to be useful. In figure 9(*b*), we show the maximum stretching rate, $|\omega_i S_{ij}\omega_j|_\infty$ (i.e. the numerator of (3.4)), for colliding Lamb dipoles at resolution 1536^3. The graph of $|\omega|_\infty^3$ at the same resolution is also included for comparison. We find that $|\omega_i S_{ij}\omega_j|_\infty \sim |\omega|_\infty^3$ in the rapid growth period.

For their simulation of the antiparallel vortex problem, Hou & Li (2008) showed that

$$|\xi_i S_{ij}\omega_j|_\infty \leqslant c|\omega|_\infty \log|\omega|_\infty, \tag{3.5}$$

where $\xi_i \equiv \omega_i/|\omega|$ and c is a constant. Given the evolution equation for $|\omega|$ and given that $|\xi_i S_{ij}\omega_j|_\infty$ bounds the value of $|\xi_i S_{ij}\omega_j|$ at the point where $|\omega|$ is maximal, this inequality implies that no singularity can occur at finite time. In our case, we have $|\omega_i S_{ij}\omega_j|_\infty \sim |\omega|_\infty^3$. If $|\omega_i S_{ij}\omega_j| \sim |\omega|^3$ where $|\omega|$ is maximal, then singularity would result; however, our relationship does not guarantee this since $|\omega_i S_{ij}\omega_j|$ may have its maximum at a point other than that where $|\omega|$ is maximal. Thus, we can only say that our relation is not inconsistent with the formation of a FTS. We can add, however, that although the position of the maximum of $|\omega_i S_{ij}\omega_j|$ and the position of the maximum of $|\omega|$ do not always coincide and their separation fluctuates, there is a good deal of correlation in these positions after $t = 2.69$.

Since we cannot resolve the evolution right up to t_s, the data can always be made to satisfy inequality (3.5) by choosing the constant c sufficiently large. However, the interesting thing to check is whether the growth of $|\omega_i S_{ij}\omega_j|_\infty$ is slower than that of $|\omega|_\infty^2 \log|\omega|_\infty$ during the period of rapid amplification. Figure 9 shows that this is far

https://doi.org/10.1017/jfm.2011.430 Published online by Cambridge University Press

from the case, and, therefore, the bound on the growth of vorticity set by Hou & Li (2006, 2008) does not seem to be relevant to our data.

Hou & Li (2006, 2008) show evidence that there is no FTS for their perturbed antiparallel vortices, while, in contrast, our data continue to support the tendency toward a FTS as resolution is increased in our simulations of colliding Lamb dipoles. Although this difference may be due to the method of filtering that Hou & Li (2006, 2008) use, it is much more likely due to the different choice of initial conditions. This is a strong indication that a pair of colliding Lamb dipoles is a better choice for an initial condition that would lead to a finite time blow-up than a pair of antiparallel vortices. We must note though that there is evidence that the initial condition based on antiparallel vortices as defined by Kerr (1993) may still lead to a singularity (Bustamante & Kerr 2008).

4. Results: Navier–Stokes

4.1. *Enstrophy evolution*

We next turn to the question of whether the Navier–Stokes equations can exhibit a singularity at high Reynolds number. Until recently, the practical resolution of numerical simulations was too low to reproduce all of the relevant events leading to turbulent flow (Brachet *et al.* 1983; Bell & Marcus 1992). Now, however, well-resolved simulations are possible, and we present such results for the case of colliding Lamb dipoles here for the first time. It should be expected that there will be little difference from the inviscid evolution in the early phase of the dipole interaction. Significant differences occur as steep gradients of vorticity form. Since Laplacian viscosity is more effective for small scales than for large, the large-scale structures can be expected to evolve as in the inviscid case, at least for some time. That is, we expect viscous effects to be felt first at the smallest scales and only later at larger scales. The main dynamical difference between viscous and inviscid flow is vortex reconnection, a phenomenon which has been analysed in great detail in the literature, with focus on the singularity issue recently given by Kerr (2001).

The evolution of energy $q = \langle u_i^2 \rangle / 2$ and enstrophy can be written as

$$\frac{\mathrm{d}q}{\mathrm{d}t} = -\frac{\Omega}{Re}, \quad \frac{\mathrm{d}\Omega}{\mathrm{d}t} = P_\Omega - \frac{D_\Omega}{Re}, \tag{4.1}$$

where $D_\Omega/Re = \langle (\partial\omega_j/\partial x_i)^2 \rangle / Re$ is the rate of enstrophy dissipation. According to the energy equation, where the right-hand side is negative definite, the energy must decay monotonically in time. By following Kolmogorov phenomenology (cf. Frisch 1995), the turbulent kinetic energy should decay in time and, after a rearrangement of energy among the different scales, the energy decay rate should be independent of the viscosity. If this is the case, the ratio on the right-hand side of the energy equation must become independent of Re for large Re. Thus, larger Re would correspond to higher enstrophy. It is more difficult to say something definite about the enstrophy evolution from these equations due to the competing effects of P_Ω and D_Ω/Re. However, we can speculate that the early behaviour will be as in the inviscid case, with the evolution of Ω driven by enstrophy production. Whether enstrophy dissipation can be sufficient to avoid singular growth of Ω for all Re is the main question.

Numerical simulations can be used to help shed light on this problem by allowing us to understand the tendency as the Reynolds number is increased. The Navier–Stokes simulations of the colliding dipoles need to be run longer than the corresponding Euler simulations because there is no clear singularity time in these simulations. A first set

https://doi.org/10.1017/jfm.2011.430 Published online by Cambridge University Press

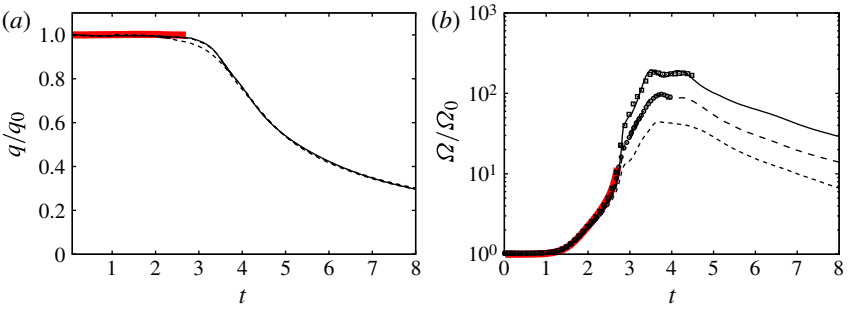


FIGURE 10. (Colour online) History of kinetic energy and enstrophy. (*a*) Energy: inviscid 1536^3, thick red line; $Re = 10\,000$ ($L_1 = 2\pi$), black solid line; $Re = 2500$ ($L_1 = 2\pi$), dashed line. (*b*) Enstrophy: inviscid 1536^3, thick red line; $Re = 10\,000$ ($L_1 = 2\pi$), solid black line; $Re = 10\,000$ ($L_1 = 4\pi$), □; $Re = 5000$ ($L_1 = 2\pi$), long dashed line; $Re = 5000$ ($L_1 = 4\pi$), ○; $Re = 2500$ ($L_1 = 2\pi$), short dashed line.

of simulations has been performed in domains of size $2\pi \times \pi \times \pi$, equal to that used for the Euler equations. This domain size is satisfactory for dipoles interacting for times not much greater than the t_s for inviscid flow. For a longer interaction, the parts of the two dipoles that are far from the collision region continue to propagate and soon leave and re-enter the periodic domain. To avoid this complication, we repeat some of the simulations in a box $4\pi \times \pi \times \pi$. It has been found that, with $L_1 = 4\pi$, the evolution up to $t = 3.0$, does not differ from that with $L_1 = 2\pi$, and between $t = 3$ and $t = 5$ there are small but not substantial differences. To have simulations completely unaffected by the periodicity, L_1 should be increased further, but this is computationally too expensive. We present data from several simulations at different Reynolds numbers: $Re = 2500$, 5000 and 10 000. For the smaller two values of Re, the type of unphysical scales that would be due to insufficient resolution are absent. For $Re = 10\,000$, there is some growth in unphysical scales, but as we shall see, the energy in those scales remains negligible.

As expected, the history of the kinetic energy (figure 10*a*) shows that for the inviscid case (red line) q is nearly constant up to the singularity time $t_s = 2.79$. For $Re = 10\,000$, the energy is nearly constant during the approach of the dipoles. As the collision occurs, the energy begins to decay rapidly. The behaviour of the energy for $Re = 5000$ is nearly identical to that shown for $Re = 10\,000$, at least they cannot be distinguished on the scale of this plot, and so a curve for $Re = 5000$ has not been drawn. At $Re = 2500$ (dashed line), some decay can be seen even during the approach of the dipoles, but even at this Re significant energy decay does not occur until the dipoles collide. The evolution of the spectra clarify that the early decay at $Re = 2500$ is associated with the formation of an exponential range. Figure 10(*a*) shows only data from simulations with $L_1 = 2\pi$. Simulations with $L_1 = 4\pi$ produced essentially identical results.

Figure 10(*a*) shows a t^{-m} power-law decay of the energy in the last period of evolution. The decay law appears to be independent of Re, suggesting that the energy containing scales are the most important scales in determining the values of the m exponent (cf. George 1992). The calculated value $m = 1.2$ agrees approximately with that measured in wind tunnel experiments where the turbulence is produced with grids of square cells made of intersecting rods of square cross-section (Lavoie *et al.* 2007).

https://doi.org/10.1017/jfm.2011.430 Published online by Cambridge University Press

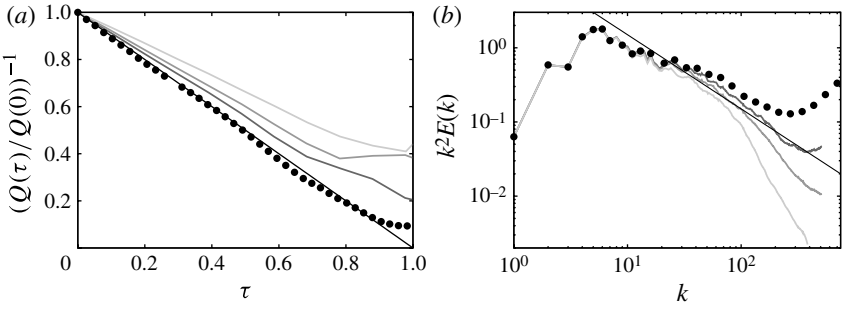


FIGURE 11. (*a*) History of $Q = P_\Omega/\Omega$ versus $\tau = (t - t_i)/(t_s - t_i)$, ($1 - \tau$: thin black line). (*b*) Enstrophy spectra at $t = 2.78$ (k^{-1}: thin black line). In both figures: $Re = \infty$, resolution 1536^3, ●; $Re = 10\,000$, 1024^3, dark grey; $Re = 5000$, 1024^3, medium grey; $Re = 2500$, 768^3, light grey.

This may suggest that the interactions of the dipolar vortices shed by such grids are similar to that in our colliding dipole problem.

The history of Ω in figure 10(*b*) is more interesting than that of the energy because several phases can be distinguished. For $t < 1$, while the dipoles are well separated and have not begun to interact, the enstrophy remains constant. Then there is a period of exponential growth ($1.8 \lessapprox t \lessapprox 2.4$), which occurs in both inviscid and viscous simulations. In the inviscid enstrophy equation exponential growth results from production such that $P_\Omega = C_\Omega \Omega$. The constant C_Ω is the enstrophy growth rate, and for the inviscid curve shown here, we have $C_\Omega \approx 0.75$. For the finite Re curves, this value decreases slightly with decreasing Re. It is during this period of time that vorticity sheets form (Orlandi & Pirozzoli 2010). Then in the period $2.6 \lessapprox t \lessapprox 2.7$, there is rapid enstrophy amplification and the physical regions where energy and enstrophy are concentrated shrink. For $\nu = 0$, this is the period that seems to lead to a FTS. If the viscosity prevents a FTS, its damping effect should modify the amplification phase characteristic of the inviscid case. To show the differences between Euler and Navier–Stokes equations during the rapid amplification phase, the previous analysis for Ω/P_Ω (figure 4*a*) is repeated here. If a FTS does occur with viscosity, we may suppose that the first effect of the viscosity for the Navier–Stokes equations, is to delay its occurrence. We check this by plotting $(\Omega/P_\Omega)(t)/(\Omega/P_\Omega)(t_i)$. Figure 11(*a*) indeed shows that extrapolating from the amplification period would give an estimated singularity time that decreases toward the inviscid result as Re increases. From figure 10(*b*), it is also clear that for each Re there is a maximum for Ω. There is no proof that for any ν there is a maximum of $\Omega(t)$. From figure 10(*b*), the trend is that the maximum of $\Omega(t)$ increases approximately linearly with Re and that the time at which $\Omega(t)$ achieves its maximum tends toward the inviscid t_s with increasing Re. There is no reason to suspect from the data that we have so far that this trend will not continue for all Re.

It is also interesting that the location of the maximum of Ω decreases toward the inviscid $t_s = 2.79$ as Re increases. From figure 11(*a*), we see that the linear trend toward the FTS for $\nu = 0$ ends at $\tau = 0.9$, that is at $t = 2.77$, just before t_s. This deviation is due to a lack of resolution. This can be deduced from figure 11(*b*) where the inviscid enstrophy spectrum at time $t = 2.78$ has developed a large pile-up at the highest wavenumbers indicating a significant amount of unphysical vorticity. For the viscous simulations, the deviation in figure 11(*a*) from FTS behaviour, leads to an end

https://doi.org/10.1017/jfm.2011.430 Published online by Cambridge University Press

of the rapid growth phase with Ω reaching a finite maximum just after the inviscid t_s. This saturation is a direct result of viscous effects, not lack of resolution. This is verified by checking the enstrophy spectra $k^2E(k)$ at $t = 2.78$, a time just before t_s. The enstrophy spectra in figure 11(*b*) show that, at the enstrophy containing scales $k \approx 10$, the k^{-3} range is the same as in the inviscid case. For $20 \lessapprox k \lessapprox 100$ the slope of the spectra increases with increasing Re. The fall-off of enstrophy at high k for $Re = 2500$ and $Re = 5000$ indicates adequate resolution. The small curl up at the end of the $Re = 10\,000$ spectrum, with an amount of enstrophy associated with the smallest scales almost 10 times smaller than in the enstrophy containing scales, indicates that the resolution at that Re is marginal.

The history of enstrophy production P_Ω and dissipation D_Ω/Re provides us with a qualitative and global picture of the collision of the dipoles. The evolution of these terms, which appear in (4.1), is shown in figure 12 for an inviscid simulation and for simulations with three different Re. During a short period after $t = 0$, P_Ω and D_Ω/Re are small relative to the values they will achieve, and $P_\Omega < D_\Omega/Re$. Note that during this period, all of the production curves coincide. Only the inviscid (black dots) and $Re = 2500$ (thick grey curve) curves are visible during this period because they overlie the two higher Re production curves. The three dissipation curves (thin lines) are, however, well separated. Since both production and dissipation remain small during this period, there is little change to the structure of the dipoles. When the dipoles get close to each other and their vortical structures start to be modified, at $t \approx 0.5$, enstrophy production becomes larger than enstrophy dissipation. From $t = 0$ until $t \approx 2.5$, there is no significant difference between the inviscid and viscous simulations with regard to production. On the other hand, the dissipation D_Ω/Re does depend on Re. Since D_Ω/Re remains small during this period, it does not significantly modify the vortex structure compared with the inviscid case; otherwise, P_Ω, which is a function of vortex structure, would develop dependence on Re. Looking at the zoomed inset in figure 12, we see that for $2.6 \lessapprox t \lessapprox 2.7$, enstrophy dissipation D_Ω/Re is independent of Re. This implies that at this time vorticity gradients as measured by the integral D_Ω must be steeper the higher the value of Re. The inset also shows that for $t \gtrapprox 2.5$ inviscid production deviates from that in the viscous simulations, and that P_Ω then shows dependence on Re. The inset also shows that after the estimated inviscid $t_s = 2.79$ for each Re the growth of P_Ω and D_Ω/Re almost stops and they approach near equilibrium with $P_\Omega \approx D_\Omega$. Note that the higher the value of Re the higher the value of P_Ω. It is interesting that from $t = 0$ until $t \approx 2.7$ the dissipation D_Ω/Re decreases as Re increases (i.e. as ν increases), and that this relationship then reverses with D_Ω/Re increasing as Re increases (i.e. as ν decreases) after $t \approx 2.7$. This inversion of the relation between D_Ω/Re and Re at $t \approx 2.7$ is necessary to allow equilibration between P_Ω and D_Ω/Re since P_Ω increases with Re.

It is very interesting that after $t \approx t_s$, enstrophy production and dissipation have achieved an approximate equilibrium in which D_Ω/Re increases with Re. This can be explained with Kolmogorov phenomenology (Frisch 1995) that implies that the velocity gradients increase when the viscosity decreases in such a way as to make the rate of energy dissipation $\varepsilon = 2\nu\Omega$ independent of ν for large Re (the law of finite energy dissipation). Figure 13(*a*) shows that after $t \approx t_s$, the energy dissipation ε becomes independent of Re. The degree to which D_Ω varies with Re is related to the fact that ε becomes independent of ν, which implies Ω becomes inversely proportional to ν. In recent high-resolution high-Re simulations Ishihara *et al.* (2007) confirmed that the energy dissipation rate is limited and does not vary with Re in statistically stationary forced isotropic turbulence. In the present colliding dipole

https://doi.org/10.1017/jfm.2011.430 Published online by Cambridge University Press

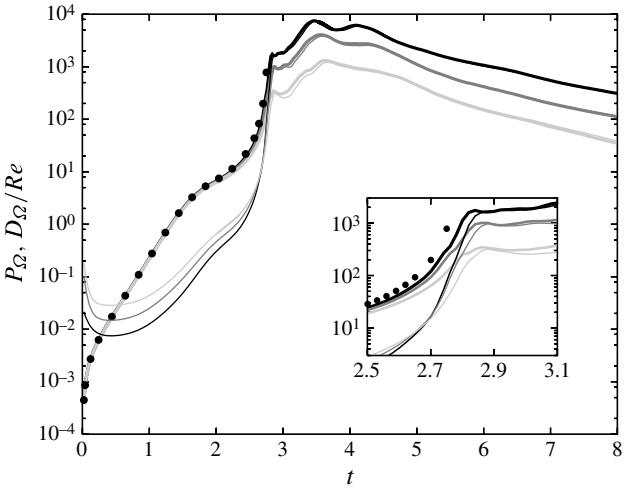


FIGURE 12. History of P_Ω (thick lines) and D_Ω/Re (thin lines): black curves, $Re = 10\,000$; dark grey curves, $Re = 5000$; light grey curves, $Re = 2500$. ●, P_Ω from the inviscid simulation with resolution 1536^3.

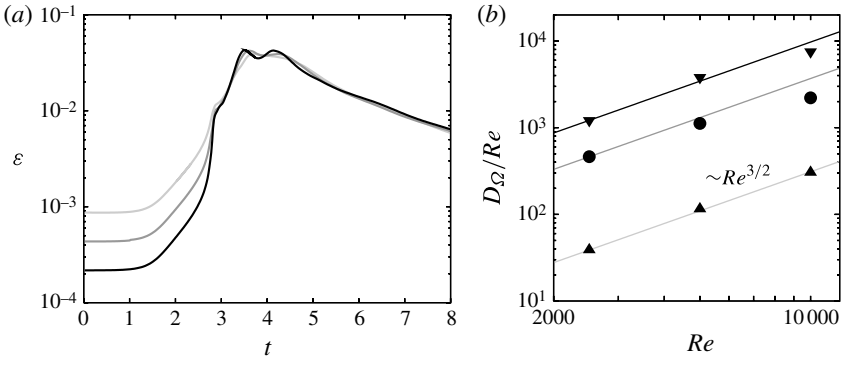


FIGURE 13. (*a*) History of $\varepsilon = 2\nu\Omega$ for colliding dipoles with $Re = 10\,000$ (black curve), $Re = 5000$ (dark grey curve) and $Re = 2500$ (light grey curve). (*b*) D_Ω/Re versus Re at $t = 5$ (●), at $t = 8$ (▲) and the peak values of D_Ω/Re over all time versus Re (▼). The straight lines represent the $Re^{3/2}$ law starting from the leftmost data point on each curve.

simulations, the energy and the rate of energy dissipation decrease after $t \gtrapprox 4.2$, but, just as in stationary forced isotropic turbulence, ε is independent of Re. For isotropic turbulence, we can write

$$D_\Omega = \int_{k_\ell}^{k_\eta} k^4 E(k)\,\mathrm{d}k. \tag{4.2}$$

Assume a model spectrum that follows the Kolmogorov spectrum $E(k) = C_K \varepsilon^{2/3} k^{-5/3}$ for $k_\ell < k < k_\eta$, where $k_\ell = 1/\ell$ and $k_\eta = 1/\eta$. Here ℓ is the integral scale and η is the Kolmogorov dissipation scale. For $k_\ell \ll k_\eta$ we then have

$$D_\Omega = \tfrac{3}{10} C_K \varepsilon^{2/3} {k_\eta}^{10/3}. \tag{4.3}$$

https://doi.org/10.1017/jfm.2011.430 Published online by Cambridge University Press

For high Re, we have $k_\eta \sim k_\ell Re^{3/4}$ (Frisch 1995). Thus, since ε and ℓ are independent of Re for large Re, we have $D_\Omega \sim Re^{5/2}$ or

$$D_\Omega/Re \sim Re^{3/2}. \tag{4.4}$$

Examining the peak values of D_Ω/Re in figure 12 (near $t = 3.6$), we find they roughly follow this law as shown in figure 13(*b*). Along with the peak values of D_Ω/Re versus Re, we also show the values of D_Ω/Re at times $t = 5$ and $t = 8$. For $Re = 2500$ and $Re = 5000$, the better resolved runs, the agreement with this 3/2 rule is good at all times shown. For $Re = 10\,000$ the agreement is good at $t = 8$ but not at $t = 5$. This is probably related to the fact that there is not enough resolution at $Re = 10\,000$ for the spectrum to contain the full exponential range, which is assumed in the theory leading to the 3/2 rule.

Although not clearly visible on the scale of figure 12, P_Ω and D_Ω do not become perfectly equal after $t = t_s$. Closer study of the relative values shows that $P_\Omega > D_\Omega$ until $t \approx 3.5$. For the period $3.5 \lessapprox t \lessapprox 4.2$ the relation between P_Ω and D_Ω oscillates in a manner that depends on Re. For $t \gtrapprox 4.2$, $P_\Omega < D_\Omega$. It is in this last period that the energy spectrum develops a $k^{-5/3}$ inertial range and a dissipation range.

4.2. *Energy spectra*

Figure 13 demonstrated that after $t \approx t_s$, ε becomes approximately independent of Re. However, a closer examination of this period shows some interesting oscillations in ε with time and some small variation with Re that is worth exploring. To emphasize these aspects, we plot ε during this period on a linear scale in figure 14(*a*). The continuous lines are from the simulations with $L_1 = 2\pi$ for $Re = 2500$, 5000 and 10 000. There are oscillations in ε which become more pronounced as Re increases. The data points marked by open circles are from a simulation with $L_1 = 4\pi$ and $Re = 10\,000$. Note that the oscillations are very much reduced compared with the $L_1 = 2\pi$ simulation at the same Re. This suggests that the oscillations are directly related to the reentry of parts of the dipoles due to the periodic boundary conditions. With the data from the $L_1 = 4\pi$ simulation, we see that after the first peak in ε, there is a relatively flat period before decay begins at $t \approx 4.3$. The decaying period corresponds to the power-law (t^{-m}) decay of the energy that is typical of isotropic turbulence as discussed above.

The evolution of ε can be directly related to changes in the enstrophy spectrum. Figure 11(*b*) shows the enstrophy spectrum at $t = 2.78$, just before the estimated inviscid t_s. The high wavenumbers show a small range of power-law scaling before falling off (or curling up in the inviscid case) at the highest wavenumbers. The power law varies with Re reaching k^{-1} (corresponding to a k^{-3} energy spectrum) in the inviscid case. In the range from $k = 1$ to $k \approx 20$, the spectrum is independent of Re for the high values of Re shown here. The later history of the spectrum is shown in figures 14(*b–f*) with time increasing from $t = 3$ in increments of $\Delta t = 0.5$. At $t = 3$ (figure 14*b*), the power-law exponent n of the energy spectrum $\propto k^n$ has increased from $n = -3$ (as in figure 11*b*) to $n = -2.5$. This is related to a change in the vortical structures resulting from vortex reconnection, a phenomenon characteristic of viscous flows. The wide power-law range at $Re = 10\,000$ and $Re = 5000$ persists at $t = 3.5$ (figure 14*c*) while the value of the exponent has increased to $n = -2$. The comparison between this simulation and one with a 768^3 resolution shows that the small energy pile-up at the end of the spectrum does not modify the shape of the enstrophy containing structures. The pile-up acts as a subgrid-model dissipating the necessary amount of energy. At $t \approx 3.5$ there is a peak in ε in figure 14(*a*). This peak cannot be attributed to the pile-up at high k for the $Re = 10\,000$ spectrum in figure 14(*c*), because such a peak also occurs in ε for $Re = 5000$, and the spectrum

https://doi.org/10.1017/jfm.2011.430 Published online by Cambridge University Press

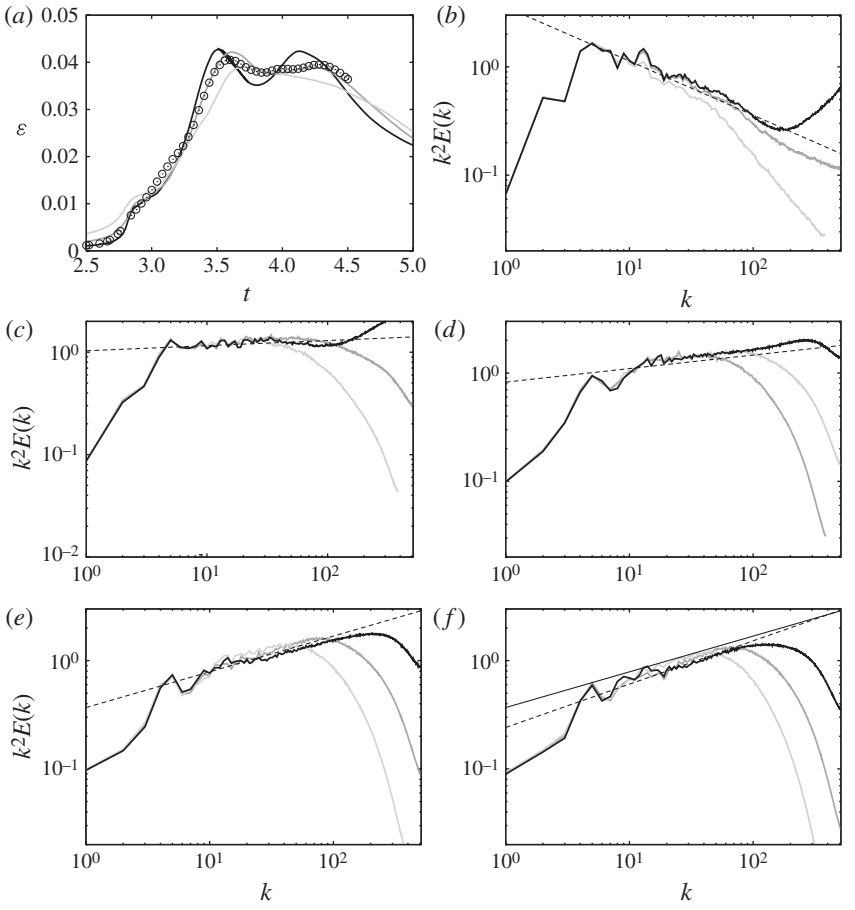


FIGURE 14. (*a*) History of ε for the viscous simulations. For this and all other panels in this figure, the thick curves are from simulations with $L_1 = 2\pi$ with one of three values of Re: $Re = 10\,000$ (thick black curve), $Re = 5000$ (thick dark grey curve) and $Re = 2500$ (thick light grey curve). The open circles are ε for $Re = 10\,000$ with $L_1 = 4\pi$. (*b–f*) Enstrophy spectra at times: (*b*) $t = 3.0$ (the additional thin dashed is $k^{-1/2}$), (*c*) $t = 3.5$ (thin dashed $k^{0.05}$), (*d*) $t = 4.0$ (thin dashed $k^{1/4}$), (*e*) $t = 4.5$ (thin dashed $k^{1/3}$), (*f*) $t = 5.0$ (thin solid $k^{1/3}$, thin dashed $k^{2/5}$).

for $Re = 5000$ has no such pile-up, but instead exhibits an exponential fall-off at high wavenumbers.

Figure 14(*d*) shows that an exponential range forms at for each Re and that the value of the exponent of the power law is increasing towards $n = -5/3$, which is reached at $t = 4.5$ (figure 14*e*). At this time there is strong dissipation at all scales. At $t = 5$ in figure 14(*f*) the exponent of the power law is about $n = -8/5$. For $t \gtrapprox 5$ both energy and enstrophy are decaying, and since the value of Re_λ is then relatively low, the power-law exponent in 14(*f*) approaches the value $n = -3/2$ that has often been observed in DNSs of forced and decaying isotropic turbulence at low Re.

4.3. *Vortical structures*

Since pressure gradients must provide the centripetal acceleration needed for highly curved flow, low pressure is located in regions of strong vorticity. Thus, visualization

https://doi.org/10.1017/jfm.2011.430 Published online by Cambridge University Press

of p can be used to define the shape of the vortical structures and to follow their evolution. The vorticity and rate of strain fields provide additional information about the structure of the vortices. By taking the divergence of the Navier–Stokes equation, it can be shown that these fields are related by $\nabla^2 p = \omega_i^2/2 - S_{ij}^2$. Cadot, Douady & Couder (1995) point out that the low pressure region along the axis of the vortex results from having the vorticity concentrated in the core of the vortex, while dissipation ($\propto S_{ij}^2$) is distributed around it. They used the tendency of bubbles to collect in low-pressure regions to successfully visualize coherent small-scale vortical structures in a laboratory experiment by using a sophisticated visualization technique. In numerical simulations, having available both ω_i and S_{ij}, the detection of the relevant vortical structures is easy. For interacting dipoles, three-dimensional contours of pressure surfaces were presented by Orlandi & Carnevale (2007) for $\nu = 0$; here, those results are compared with the present results for $\nu \neq 0$. For the simulation with $Re = 2500$, at $t = 2.5$, just before the beginning of the period of strong vorticity amplification, isosurface plots in figure 15(*a*) of p (blue) and $u_i^2/2$ (yellow) give an indication of the perturbed shape of the vortex tubes that have become intertwined during the interaction. In the same figure, the most intense vorticity $\omega_i^2/2$ is distributed around the point of interaction of the primary vortex tubes (the yellow and blue structure). From the isosurfaces in figures 15(*a*) and 15(*b*), it is difficult to understand how pressure, energy and enstrophy density are related. In figure 15(*c*), contour plots of p (blue), $u_i^2/2$ (yellow) and $\omega_i^2/2$ (blue) in a $x_1 - x_3$ cross-section at the location of high enstrophy density show their spatial distribution and relationships more clearly. Here we see that in the viscous case at $t = 2.5$, the pressure minima coincide approximately with the maxima of $\omega_i^2/2$ and that the peak of energy is located in a region of weak $\omega_i^2/2$. At this time the vorticity is most intense in the two tubular structures that in figure 15(*b*) surround the region of interaction, where the dipoles by mutual induction bend the central part of the two dipoles so that they come close to each other. As a result, a single structure forms. This structure is indicated by the blue and yellow surfaces in figure 15(*b*). In the region of very high levels of $\omega_i^2/2$ shown in red in figure 15(*a*), there are four structures. There are two thin tubular structures visible on the lower side of the thick primary vortices. There are also two sheet-like structures on the upper forward side of the primary vortices, that appear connected in this view but are in fact two separate structures. The size of these small high-vorticity regions increases as viscosity is reduced. The two tubular structures become very strong and large in the inviscid case (figures 15*b* and 15*d*). A low-pressure region forms in their interior (figure 15*c*). Orlandi & Carnevale (2007) showed that the intense vorticity amplification occurs in the vortex sheets and not in the vortex tubes. These sheets are not visible in figure 15(*b*) because they are obscured by the large encircling intense vortex tubes (also in red); however, they are located in the same position as those in figure 15(*a*). They have high enstrophy density, which increases with increasing Reynolds number. Figure 15(*d*) shows the distribution of ω_i^2 and S_{ij}^2 in the sheet-like structures that were mentioned above. Here the surfaces of high S_{ij}^2 and ω_i^2 are very close together, in part lying right on top of each other. This is very different from the case of a vortex tube of circular cross-section where typically ω_i^2 is high at the centre of the core of the vortex and low outside the core, while S_{ij}^2 is only high outside the core. The geometric coincidence of overlapping high ω_i^2 and S_{ij}^2 zones is the reason why rapid vorticity amplification occurs within the sheet-like structures. This finding is consistent with the observations made by Kerr (1993) and Hou & Li (2006) that points where singular behaviour manifests itself are typically associated

https://doi.org/10.1017/jfm.2011.430 Published online by Cambridge University Press

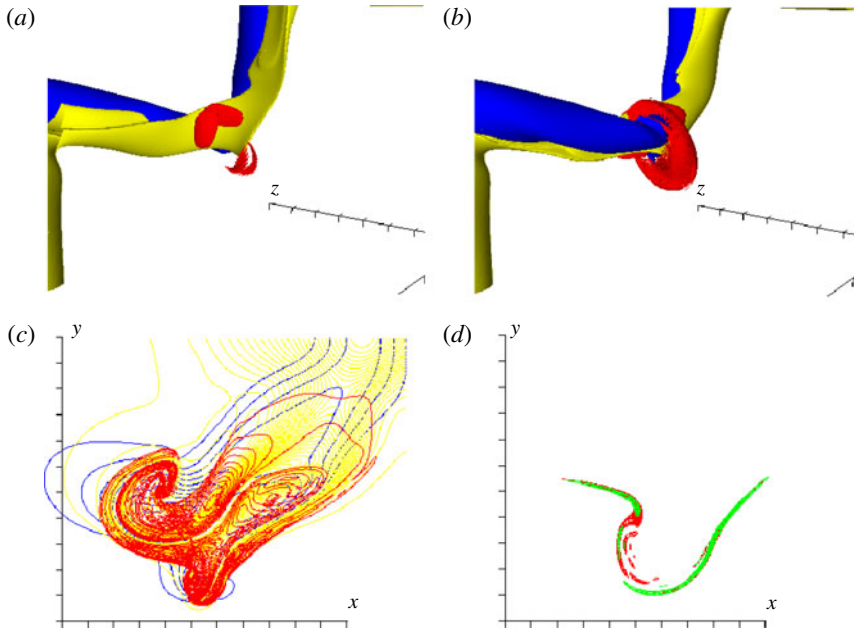


FIGURE 15. (*a*) Isosurfaces of $p = -4$ (blue), $u_i^2/2 = 6$ (yellow) and $\omega_i^2/2 = 900$ (red) at $t = 2.5$ for $Re = 2500$. (*b*) As in (*a*) but for inviscid flow. (*c*) Contour plots for the inviscid flow at $t = 2.5$ in a plane $x_1 - x_3$ (at $x_2 = 0$): p with $\Delta = -0.5$ (blue); $u_i^2/2$ with $\Delta = 0.25$ (yellow) and $\omega_i^2/2$ with $\Delta = 100$ (red). (*d*) As in (*c*) but for $\omega_i^2/2$ (red) and S_{ij}^2 (green) with increment $\Delta = 250$ starting from a value equal to 1250 (resolution 768^3). In (*a*) and (*b*) $z = x_3$. In (*c*) and (*d*) $x = x_1$ and $y = x_3$, in (*c*) $x_{min} = -1.0, x_{max} = 1.2, y_{min} = -2.2, y_{max} = 0$, in (*d*) $x_{min} = -0.4, x_{max} = 0.4, y_{min} = -2.1, y_{max} = -1.3$.

with the roll-up of the edge of a vortex sheet. Curved vortex sheets were also observed near the singularity time by Orlandi & Carnevale (2007), and were analysed in more detail by Orlandi (2009), see figure 7 in that paper, where two curved vortex sheets of small lateral size wrap around the region where the FTS should occur. The vortex lines emanating from that region are not smooth, just as should be expected in regions of strong vorticity amplification.

The flow visualizations in figure 15 were obtained from simulations of resolution 768^3, which is insufficient to get a clear view of the dynamics of the enstrophy containing scales as we get closer to the inviscid $t_s = 2.79$. We have now doubled the resolution and will visualize the flow at $t = 2.75$. No matter how high the resolution, there is always some build up of unphysical scales the closer we get to $t = t_s$. For resolution 1536^3, we see such a build-up in figure 11(*b*) for $400 \lessapprox k$. Unphysical structures at these scales may contaminate the visualizations, as well as the enstrophy p.d.f.s shown in figure 7. To eliminate the contribution of this last part of the spectrum, the velocity field is filtered by spectral truncation at $k = 400$ before visualizing the physical-space fields. The vortex dynamics in the region between the two dipoles is emphasized by zooming in on the central region at $t = 2.75$. Figure 16(*a*) shows that the high levels of energy (yellow isosurface) are associated with the original but now deformed vortex tubes and also with the thin tubular and curved sheet-like structures of high vorticity (red). The most intense vorticity amplification occurs in the regions of high curvature in the two thin curved vortex sheets (red), and not in the two thin

https://doi.org/10.1017/jfm.2011.430 Published online by Cambridge University Press

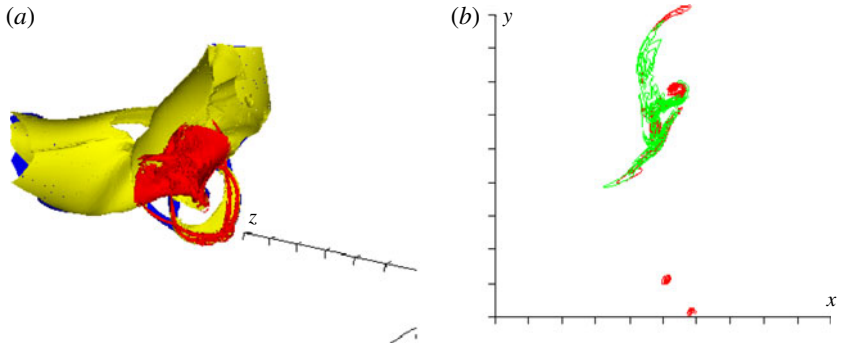


FIGURE 16. Results from an inviscid simulation with resolution 1536^3. (*a*) Isosurfaces at $t = 2.75$ of: $p = -16$ (blue), $u_i^2/2 = 24$ (yellow) and $\omega_i^2/2 = 500$ (red). (*b*) Contour lines in an $x_1 - x_3$ plane at $x_2 = 0$, $\omega_i^2/2$ (red) and S_{ij}^2 (green) with increment $\Delta = 12\,500$ starting from a value equal to 25 000, (*b*) is zoomed in on the area of interest and $x = x_1$ and $y = x_3$. In (*a*) $z = x_3$.

red vorticity tubes. This can be better appreciated through contour plots in $x_1 - x_3$ cross-sections at $x_2 = 0$ (figure 16*b*). The filamentary red (ω_i^2) and green (S_{ij}^2) elongated structures correspond to the vortex sheet-like structures of (*a*). The large circular red dot in the cusp of the green sheets corresponds to the point where the vortex sheets are rolling up. The strongest amplification of vorticity occurs where the vorticity and rate of strain fields are strong and overlap, a necessary condition for rapid vortex stretching. This condition is met here in the vortex sheet, but not in the vortex tube that is rolling up. Inside the tube, the rate of strain is small, while it may be surrounded by a region of high rate of strain. The two small red dots in the lower portion of (*b*) correspond to the two thin red tubular vortices shown in (*a*). The rate of strain field for these thin tubes is weak even outside the tubes, at least relative to the high rate of strain values found in the sheets. Thus, the FTS, if it occurs, will lie in the sheets and not in the vortex tubes.

At $t = 2.78$, which is close to t_s, the same energy spectra $E(k)$ that were used to prepare the enstrophy spectra shown in figure 14(*b*) are replotted in figure 17(*a*) as compensated spectra: $k^3E(k)$. This figure shows that at the large scales, approximately $k < 100$, the energy spectrum roughly obeys the k^{-3} power law for Re even down to $Re = 2500$. Orlandi (2009) showed that this power-law range is directly linked to the presence of the sheet-like structures described above. For $Re = 5000$ and $Re = 2500$ a dissipation range ends the power-law behaviour at higher k. The compensated spectrum for $Re = 10\,000$ obtained from the 1024^3 simulation indicates that there may be significant unphysical small-scale energy for $k \gtrapprox 400$.

With viscosity, the simulations can be allowed to run beyond the inviscid t_s. This allows us to examine the subsequent short period of time during which there is a rapid passage from the k^{-3} to the $k^{-5/3}$ energy-spectrum power law. This change in slope (figure 14*a*) can then be associated with the modifications in the vortex structures that occur during this period. Figures 13 and 14(*a*) show that from time $t = 2.78$ to $t = 3.0$, ε continues to grow but at a reduced rate. A comparison of figure 17(*a*) with figure 17(*b*), shows that the k^{-3} range disappears during this period with significant growth of $k^3E(k)$ at $k = 100$ and beyond. The enstrophy spectra at $t = 3$ in figure 14(*b*) show unphysical scales at $Re = 10\,000$ but not at the smaller Reynolds numbers. In figure 17(*b*), the power law at the large scales can be estimated

https://doi.org/10.1017/jfm.2011.430 Published online by Cambridge University Press

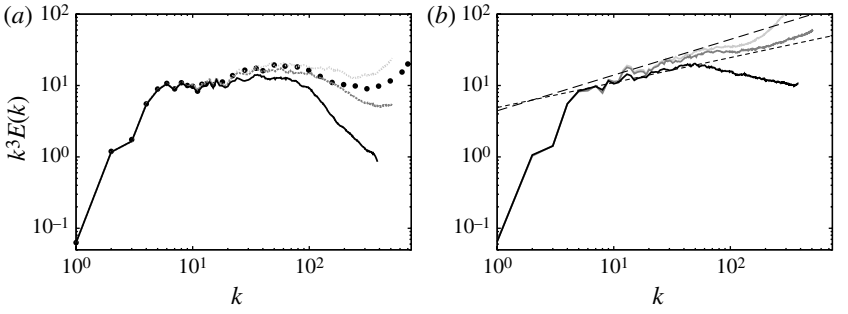


FIGURE 17. Compensated energy spectra at (*a*) $t = 2.78$ and (*b*) $t = 3.0$. The two thin lines are for $E(k) \propto k^{-2.5}$ (short-dashed) and $k^{-2.35}$ (long-dashed). ● 1536^3, inviscid; light grey curve, $Re = 10\,000$; dark grey curve, $Re = 5000$ (1024^3); black curve, $Re = 2500$ (768^3).

as $k^{-2.5}$ for $Re = 10\,000$, and $k^{-2.35}$ for $Re = 2500$. Note also that even at $Re = 2500$ the resolution used, 768^3, is not sufficient to allow an exponential range to exist at this time; however, by $t = 3.5$ a true exponential range does form as seen in figure 14.

The effect of the viscosity on the modification of the vortical structures can be analysed by using the flow fields at $Re = 10\,000$ and $Re = 2500$. The spectra at $t = 3$ in figure 14(*b*) show that 768^3 resolution is satisfactory for $Re = 2500$ but that at resolution 1024^3 for $Re = 10\,000$ there are some unphysical small scales for $200 < k$. To visualize the quantities of interest, the velocity field is filtered by truncating at $k = 200$. Figures 18(*a*) and 18(*b*) show that the energy is in large part found in the vortex tubes that made up the original dipoles, and to somewhat lesser extent in the new tubular vortical structures generated by the interaction. Comparison of figures 18(*a*) and 18(*b*) demonstrates that the energy content decreases on reducing the Reynolds number. The structures with high enstrophy are those generated in the central region where the interaction is strongest. There are both sheet-like and tube-like structures of high enstrophy. The tube-like structures have very small cross-sections relative to the sheet-like structures. Very elongated tubular structures are visible at both Reynolds numbers. They contribute to the range of wavenumbers where the spectra in figure 14(*b*) overlap. The small vortical structures visible in figure 18(*a*) but much less so in figure 18(*b*) are those contributing to the enstrophy spectra in the $40 < k < 200$ range. These structures are located in the region where for the inviscid flow at $t = 2.78$ the intense sheet-like structures form. It seems plausible that these unstable sheet-like structures generate the very small scales. At $Re = 2500$ the viscosity destroys these small scales, and figure 18(*b*) shows that tubular structures form from the roll-up of the intense sheet-like structures. The tubular structures do exist in figure 18(*a*) but are covered by the small scales with the same enstrophy content.

It is interesting to investigate how S_{ij}^2 is distributed in the vortex structures shown in figure 18. In figures 19(*a*) and 19(*b*), the surface contour of S_{ij}^2 (yellow) and $\omega_i^2/2$ (red) show that these two quantities have similar distributions that are very intertwined, although there are notable points where the fields are separated. These figures show that these two quantities are distributed at all scales, and that many more small-scales are excited at $Re = 10\,000$ than at $Re = 2500$. To determine which structures are linked to a certain range of the enstrophy spectrum shown in figure 14(*b*) at $t = 3$, the spectrum can be filtered by eliminating modes with k greater than some k_{trunc}. Figure 19(*c*) is the result of filtering with $k_{trunc} = 140$, the wavenumber where the

https://doi.org/10.1017/jfm.2011.430 Published online by Cambridge University Press

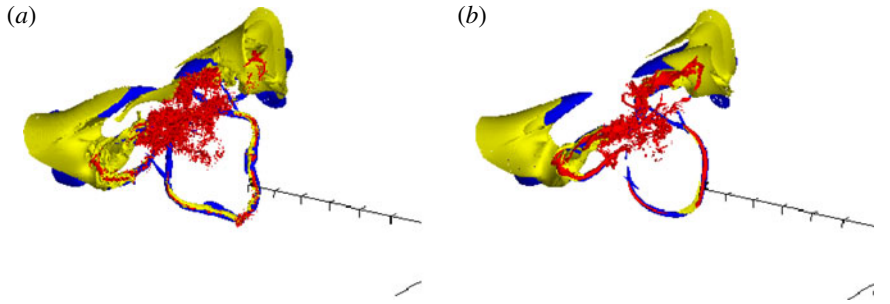


FIGURE 18. Isosurfaces: $p = -3.5$ (blue), $u_i^2/2 = 4.7$ (yellow) and $\omega_i^2/2 = 50\,000$ (red) at $t = 3.0$ for (*a*) $Re = 10\,000$ and (*b*) $Re = 2500$.

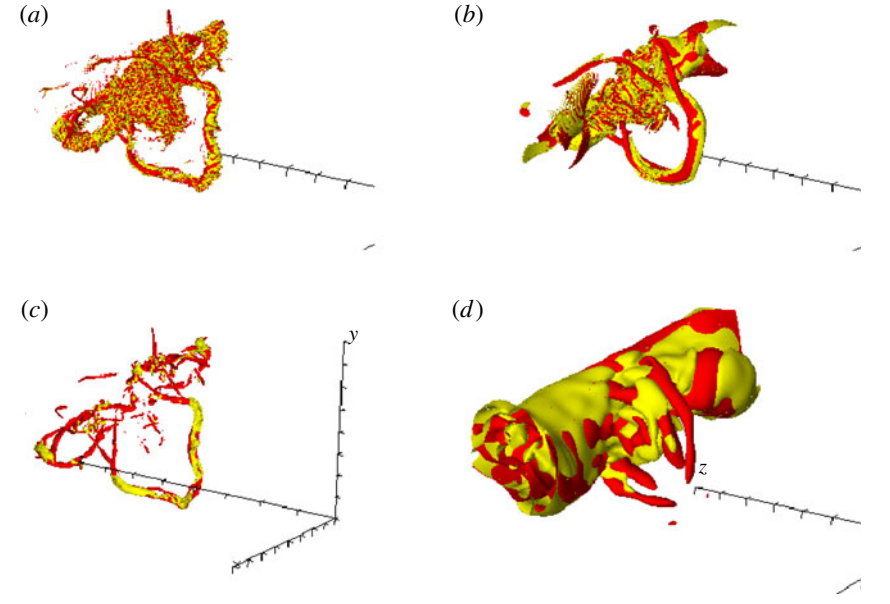


FIGURE 19. Isosurfaces of $\omega_i^2/2$ (red) and S_{ij}^2 (yellow) at $t = 3.0$. (*a*) $Re = 10\,000$ ($\omega_i^2/2 = 10\,000$, $S_{ij}^2 = 10\,000$); (*b*) $Re = 2500$ ($\omega_i^2/2 = 10\,000$, $S_{ij}^2 = 10\,000$); (*c*) $Re = 10\,000$, filtered fields with $k_{trunc} = 140$; (*d*) $Re = 10\,000$, filtered field with $k_{trunc} = 25$ ($\omega_i^2/2 = 100$, $S_{ij}^2 = 100$).

power law ends. By thus eliminating the smallest scales, including those contaminated by the effect of insufficient resolution, figure 19(*c*) shows that the high values of S_{ij}^2 and $\omega_i^2/2$ are concentrated in long thin structures. These structures are closely associated with the main primary vortex tubes that have been bent by the interaction and the long secondary structures produced by the interaction. Figure 19(*d*) is the result of filtering with $k_{trunc} = 25$. The spectra shown in figure 14(*b*), for three different *Re* are all substantially the same for $k < 15$. Thus the shape of the structures visualized with S_{ij}^2 and $\omega_i^2/2$ does not change much with *Re*.

Figure 14(*b–f*) show the evolution of the spectra for three different Reynolds number. From these alone it is difficult to understand how the vortical structures

https://doi.org/10.1017/jfm.2011.430 Published online by Cambridge University Press

change in time. The shape of the large scale structures, in which the energy is initially concentrated, is shown in figure 18 in the form of isosurfaces of p and $u_i^2/2$, while the small scales are indicated by visualizing an isosurface of $\omega_i^2/2$. In figure 18 there is a separation of small and large scales in the sense that the intense small scale associated with the red isosurface are located in the centre of the interaction region while the energy containing scales are still, at $t = 3$, located in the large-scale vortex tubes. This separation persists for a short period after t_s. However, figure 14(*c–f*) show that after $t = 3.5$ there is a transition from what we might call large-scale vortex dynamics to turbulence, corresponding to the transition from an energy spectrum with a steep power law $\approx k^{-3}$ to one with a $\approx k^{-5/3}$ spectrum. The visualizations in figure 20(*a–d*) (at the same instants of time corresponding to figure 14*c–f*) for $Re = 10\,000$, show that at $t = 3.5$ the small scales, at the centre of the figure, generated by the interaction of the two dipoles, disappear, while those in the side regions, where the energy is concentrated, survive. At $t = 3.5$ (figure 20*a*), the enstrophy isosurface (red) does not have a well-defined shape. In part, this is due to insufficient resolution, as can be observed in the enstrophy spectrum in figure 14(*c*). In contrast, flow visualizations for well-resolved flow at $Re = 2500$ (not presented) show well-defined tubular vortical structures. By $t = 4$ enstrophy pile-up at $Re = 10\,000$ has disappeared (figure 14*d*) and an exponential dissipation range has started to form. Figure 20(*b*) shows that at $t = 4$ the enstrophy is concentrated in elongated tubular structures of various sizes. These are now located within the energy containing regions. This is an indication that by this time there is a strong transfer of energy from large to small scales and that this transfer is local in physical space. At $t = 4.5$ this process is even better defined (figure 20*c*) where the direct link between the enstrophy and the energy containing scales is shown. At $t = 4.5$, and also at $t = 5$, (figure 20*d*) the energy spectrum power law is very close to the Kolmogorov $k^{-5/3}$ law. Kraichnan (1971) showed that this spectrum is associated with local energy transfer in spectral space in forced stationary isotropic turbulence. This was confirmed in DNSs of stationary forced turbulence by Domaradzki & Rogallo (1990). Crocco & Orlandi (1985), using eddy-damped quasi-normal Markovian (EDQNM) spectral closures, showed that this is also the case in decaying isotropic turbulence. In forced isotropic turbulence, energy and enstrophy are distributed throughout the whole domain, and so consequently energy transfer appears local in the physical domain as well as in the spectral domain. The colliding Lamb dipole problem, on the other hand, is very inhomogeneous. In figure 18, we saw that for $t < t_s$, much of the energy in the flow lies outside of the interaction region where enstrophy is strong and growing rapidly. If we associate the growth of enstrophy with the transfer of energy to small scales, and assume that this is the main transfer of energy, then it seems probable that the energy transfer at this time is non-local in physical space, that is energy from the extended main vortex tubes is being transferred into the localized interaction region. Given that the energy spectrum is also rather steep at this time, this is probably also a non-local transfer of energy in spectral space. After t_s, the energy spectrum tends toward $k^{-5/3}$, which at least for isotropic turbulence is associated with local energy transfer. At the same time, figure 20 shows that the distributions of energy and enstrophy become completely entangled and of similar scale, suggesting that the transfer has also become local in physical space.

5. Conclusions

The aim of this work was to better understand the differences between inviscid and viscous high-Reynolds-number flows and, in particular, to obtain some answers on the

https://doi.org/10.1017/jfm.2011.430 Published online by Cambridge University Press

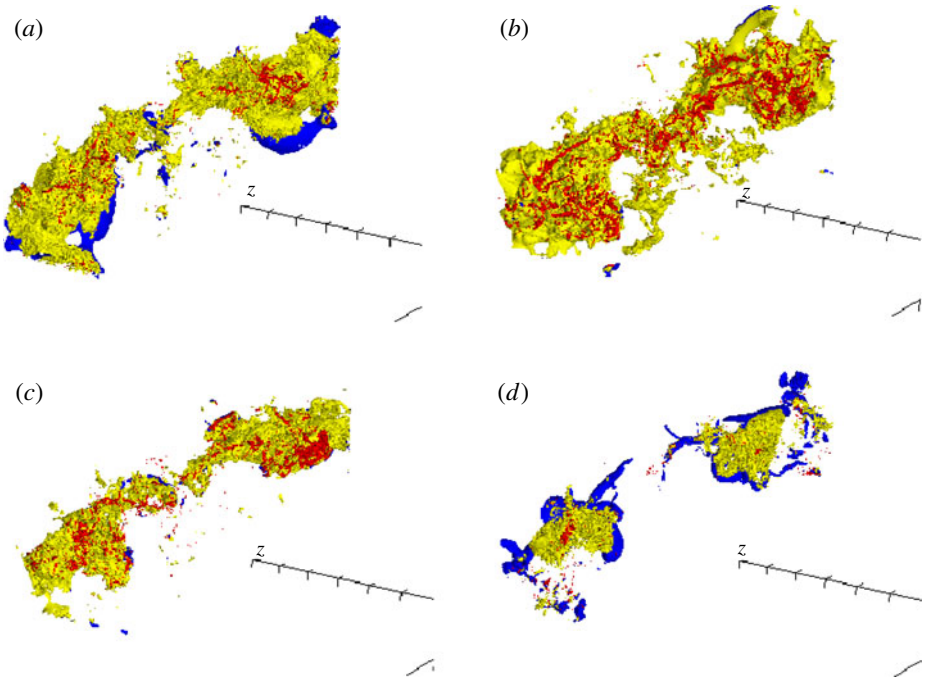


FIGURE 20. Flow visualization of surfaces of pressure p (blue), $u_i^2/2$ (yellow) and $\omega_i^2/2$ (red) for the case $Re = 10\,000$. Here p and $u_i^2/2$ are scaled by the total instantaneous energy $q(t)$ and $\omega_i^2/2$ is scaled by the total enstrophy $\Omega(t)$. The times and isosurface levels are: (*a*) $t = 3.5$, $p = -10$, $u_i^2/2 = 20$, $\omega_i^2/2 = 250$, $q = 0.200$, $\Omega = 398$; (*b*) $t = 4.0$, $p = -2$, $u_i^2/2 = 3$, $\omega_i^2/2 = 40$, $q = 0.163$, $\Omega = 347$; (*c*) $t = 4.5$, $p = -1.5$, $u_i^2/2 = 2$, $\omega_i^2/2 = 16$, $q = 0.131$, $\Omega = 281$; (*d*) $t = 5.0$, $p = -0.7$, $u_i^2/2 = 1$, $\omega_i^2/2 = 10$, $q = 0.105$, $\Omega = 176$.

question of the possible occurrence of a FTS starting from smooth initial conditions. Of course, DNSs cannot give a definite answer on the existence of a FTS, because that would require infinite resolution. However, with the limited resources at our disposal, it was possible to obtain trends which could be useful to mathematicians for their theoretical analyses, as was pointed out by Majda & Bertozzi (2002). Our results suggest that it is probable that an inviscid FTS occurs for colliding Lamb dipoles.

Showing a trend toward a FTS requires a judicious choice of both the numerical method and the initial condition. We have argued that the present second-order energy-conserving finite-difference scheme and the Lamb-dipole initial condition are appropriate choices, and we have used them in a series of simulations to investigate the differences in the trends of characteristic quantities in viscous and inviscid flows. As had been expected, we found that in the early stage of the evolution the differences between inviscid and viscous flow are minimal. The main differences appear during the period of strong vorticity amplification. The smaller the Reynolds number, the earlier the deviation from the inviscid behaviour begins. The most noticeable difference in the early evolution between inviscid and viscous flow is the effect of finite enstrophy dissipation, which at early times is dependent on Re. Changing Re changes the energy spectrum primarily at the high wavenumbers and not significantly at low wavenumbers. At $Re = 2500$ the simulation is fully resolved at all times, and a well-defined exponential dissipation range forms. This is not the case

https://doi.org/10.1017/jfm.2011.430 Published online by Cambridge University Press

at $Re = 10\,000$. For that Re, when $t \approx t_s$, the estimated inviscid singularity time, the enstrophy evolution deviates from the inviscid trend, and there is a pile-up of energy near the high-k end of the spectrum. However, after t_s this pile-up relaxes and is replaced by an exponential dissipation range.

For the colliding-dipole high-Re flow, we have seen that the energy spectrum has a tendency early on to evolve toward a k^{-3} spectrum as in the inviscid case. With viscosity, after t_s the spectrum evolves toward the shallower $k^{-5/3}$ spectrum terminated by a dissipation range. During this latter phase of the evolution, the energy dissipation rate $\varepsilon = 2\nu\Omega$ becomes independent of Re. The independence of the dissipation rate implies that the enstrophy Ω must scale as Re. The independence of ε on Re was found earlier for the decaying Taylor–Green flow (Brachet 1991; Frisch 1995). Recently, this independence has also been verified in high-resolution simulations at high Re in stationary forced isotropic turbulence (Ishihara *et al.* 2007). These results are consistent with a model for an energy spectrum that is $k^{-5/3}$ truncated by a dissipation range with $k_\eta \sim Re^{4/3}$ as discussed above in § 4. On the basis of this model spectrum, the enstrophy dissipation D_Ω/Re should scale as $Re^{3/2}$, which is in reasonable agreement with our results as shown in figure 13(*b*). Thus, our viscous simulations are consistent with the notion that there will be no singularity in viscous flow. Only in the limit of $Re \to \infty$ does $\Omega \to \infty$ by ever increasing the length of the $k^{-5/3}$ inertial range with increasing Re. This is a very different scenario from that suggested by the inviscid simulations. Rather than Ω reaching ∞ by sending k_η to ∞ with a $k^{-5/3}$ spectrum, the inviscid simulations suggest that a k^{-3} spectrum is achieved everywhere in a finite amount of time.

We have further seen that during the transition from a k^{-3} to a $k^{-5/3}$ spectrum, the physical regions of high-enstrophy values shrink. Recall that in the inviscid interaction, two sheet-like and two tubular intense vortex structures form (Orlandi & Carnevale 2007) and that it is at the point of high curvature in curved sheet-like structures that there is rapid vorticity amplification. In a fully resolved simulation this vorticity amplification produces self-similar structures as discussed by Orlandi (2009). With viscosity, the unstable sheet-like structures roll up and are rapidly dissipated. The dissipated structures do not reform, and small scales are no longer generated in this region. Instead, energy transferred to smaller scales reappears as enstrophy containing small-scale structures in regions closely linked to the energy-containing scales, which are primarily the remains of the original vortex tubes that lie somewhat outside where the strong interaction had been.

After the energy spectrum achieves a broad $k^{-5/3}$ range, characteristic of isotropic turbulent flow, the kinetic energy as well as the rate of energy dissipation begin a long decline. This decaying stage of the flow has not been analysed in detail here because to resolve all scales of the colliding Lamb-dipole problem, including the parts of the tubes that are distant from the interaction region and continue to propagate in the x_1 direction, would require a much longer domain than was computationally practical in the present high-resolution study. However, the conditions of our flow in a small box are not too different from that in isotropic turbulence periodic boundary condition simulations which involve interactions among different kinds of large-scale structures that move across the domain. Under these conditions, we have been able to estimate that the turbulent kinetic energy decays as t^{-m} with $m \approx 1.2$ for $5 < t$, in agreement with related laboratory results.

To conclude, by comparing viscous and inviscid simulations with the same initial conditions, we have been able to analyse the formation of energy spectra with long power-law ranges, to relate the slope of the power law to the interaction of the

https://doi.org/10.1017/jfm.2011.430 Published online by Cambridge University Press

vortical structures in the flow, and to study the modification of those structures caused by viscosity. Beyond this, we believe that the study of the interaction of orthogonal dipoles can help us understand the evolution of turbulence generated by a grid in wind tunnel experiments. For example, the grid considered by Lavoie *et al.* (2007) is composed of orthogonal cylinders. Each cylinder should shed vortex dipoles, and thus the flow past the grid should result in many interactions of the type considered here. Experimentally, it is rather difficult to measure the quantities analysed here. Therefore, in the near future, we intend to perform simulations to reproduce as closely as possible the experiment of Lavoie *et al.* (2007) and to verify whether the spectra and other quantities behave as was found in the present paper.

Acknowledgements

The support of a MIUR 60 % grant is acknowledged. The computer time was given by CASPUR and by CINECA. Some of the simulations were performed in a cluster acquired through a PRIN grant. GFC acknowledges support from National Science Foundation grant OCE 11-29059.

REFERENCES

BATCHELOR, G. K. 1967 *An Introduction to Fluid Dynamics*, p. 617. Cambridge University Press.

BEALE, J. T., KATO, T. & MAJDA, A. 1984 A remark on the breakdown of smooth solutions of the 3D Euler equations. *Commun. Math. Phys.* **94**, 61–66.

BELL, J. B. & MARCUS, D. L. 1992 Vorticity intensification and transition to turbulence in three-dimensional Euler equations. *Commun. Math Phys.* **147**, 371–394.

BRACHET, M. E. 1991 Direct simulation of three-dimensional turbulence in the Taylor–Green vortex. *Fluid Dyn. Res.* **8**, 1–8.

BRACHET, M. E., MEIRON, D. I., ORSZAG, S. A., NICKEL, B. G., MORF, R. H. & FRISCH, U. 1983 Small-scale structure of the Taylor–Green vortex. *J. Fluid Mech.* **130**, 411–452.

BUSTAMANTE, M. D. & KERR, R. M. 2008 3D Euler about a 2D symmetry plane. *Physica* D **237**, 1912–1920.

CADOT, O., DOUADY, S. & COUDER, Y. 1995 Characterization of the low-pressure filaments in a three-dimensional turbulent shear flow. *Phys. Fluids* **7**, 630–646.

CICHOWLAS, C. & BRACHET, M. 2005 Evolution of complex singularities in Kida–Pelz and Taylor–Green inviscid flows. *Fluid Dyn. Res.* **36**, 239–248.

CICHOWLAS, C., DEBBASHN, F. & BRACHET, M. 2006 Evolution of complex singularities and Kolmogorov scaling in truncated three-dimensional Euler flows. In *IUTAM Symposium on Elementary Vortices and Coherent Structures: Significance in Turbulence Dynamics*, pp. 319–328. Springer.

CONSTANTIN, P. 1994 Geometric statistics in turbulence. *SIAM Rev.* **36**, 73–98.

CROCCO, L. & ORLANDI, P. 1985 A transformation for the energy-transfer term in isotropic turbulence. *J. Fluid Mech.* **161**, 405–424.

DOMARADZKI, J. & ROGALLO, R. S. 1990 Local energy transfer and non-local interactions in homogeneous, isotropic turbulence. *Phys. Fluids* A **2–3**, 413–426.

DUPONCHEEL, M., ORLANDI, P. & WINCKELMANS, G. 2008 Time-reversibility of the Euler equations as a benchmark for energy conserving schemes. *J. Comp. Phys.* **227**, 8736–8752.

FRISCH, U. 1995 *Turbulence*. Cambridge University Press.

GALAKTIONOV, V. A. 2009 On blow-up twistors for the Navier–Stokes equations in R3. arXiv:0901.4286.

GEORGE, W. K. 1992 The decay of homogeneous isotropic turbulence. *Phys. Fluids* **4**, 1492–1509.

GIBBON, J. D. 2008 The three-dimensional Euler equations: where do we stand? *Physica* D **237**, 14–17.

https://doi.org/10.1017/jfm.2011.430 Published online by Cambridge University Press

GOTOH, T., FUKAYAMA, D. & NAKANO, T. 2002 Velocity field statistics in homogeneous steady turbulence obtained using a high-resolution direct numerical simulation. *Phys. Fluids* **14, 3**, 1065–1081.

HORIUTI, K. & FUJISAWA, Y. 2008 The multi-mode stretched spiral vortex in homogeneous isotropic turbulence. *J. Fluid Mech.* **595**, 341–366.

HOU, T. Y. & LI, R. 2006 Dynamic depletion of vortex stretching and non-blowup of the 3D incompressible Euler equations. *J. Nonlinear Sci.* **16**, 639–664.

HOU, T. Y. & LI, R. 2008 Blowup or no blowup? The interplay between theory and numerics. *Physica* D **237**, 1937–1944.

ISHIHARA, T., KANEDA, Y., YOKOKAWA, M., ITAKURA, K. & UNO, A. 2007 Small-scale statistics in high-resolution direct numerical simulation of turbulence: Reynolds number dependence of one-point velocity gradient statistics. *J. Fluid Mech.* **592**, 335–366.

JIMENEZ, J., WRAY, A. A., SAFFMAN, P. G. & ROGALLO, R. S. 1993 The structure of intense vorticity in isotropic turbulence. *J. Fluid Mech.* **255**, 65–90 the data are available in AGARD AR-345 1998.

KERR, R. M. 1993 Evidence for a singularity of the three-dimensional, incompressible Euler equations. *Phys. Fluids* A **5**, 1725–1746.

KERR, R. M. 2001 A new role for vorticity and singular dynamics in turbulence. In *Nonlinear Instability Analysis, Volume II* (ed. L. Debnath), pp. 15–68. WIT Press.

KERR, R. M. 2006 Computational Euler history. arXiv:physics/0607148v2 [physics.flu-dyn].

KRAICHNAN, R. H. 1971 Inertial range transfer in two- and three-dimensional turbulence. *J. Fluid Mech.* **47**, 525–535.

KOLMOGOROV, A. N. 1942 The local structure of turbulence in incompressible viscous fluid for very large Reynolds numbers. *Proc. R. Soc. Lond.* A **434**, 9–13.

LAMB, H. 1932 *Hydrodynamics*, p. 738. Cambridge University Press.

LAVOIE, P., DJENIDI, L. & ANTONIA, R. A. 2007 Effects of initial conditions in decaying turbulence generated by passive grids. *J. Fluid Mech.* **585**, 395–420.

LU, L. & DOERING, C. R. 2008 Limits of enstrophy growth for solution of the three-dimensional Navier–Stokes equations. *Indiana Univ. Math. J.* **57**, 2693–2728.

MAJDA, A. J. & BERTOZZI, A. L. 2002 *Vorticity and Incompressible Flow*. Cambridge University Press.

MAZELLIER, N. & VASSILICOS, J. C. 2010 Turbulence without Richardson Kolmogorov cascade. *Phys. Fluids* **22**, 075101.

ORLANDI, P. 2000 *Fluid Flow Phenomena: A Numerical Toolkit*. Kluwer.

ORLANDI, P. 2009 Energy spectra power laws and structures. *J. Fluid Mech.* **623**, 353–374.

ORLANDI, P. & CARNEVALE, G. F. 2007 Nonlinear amplification of vorticity in inviscid interaction of orthogonal Lamb dipoles. *Phys. Fluids* **19** (5), 057106.

ORLANDI, P. & PIROZZOLI, S. 2010 Vorticity dynamics in turbulence growth. *Theoret. Comput. Fluid Dyn.* **24**, 247–251.

PUMIR, A. & SIGGIA, E. 1990 Collapsing solutions to the 3D Euler equations. *Phys. Fluids* A **2**, 220–241.

https://doi.org/10.1017/jfm.2011.430 Published online by Cambridge University Press